HHS Public Access

Author manuscript

Curr Biol. Author manuscript; available in PMC 2022 October 11.

Published in final edited form as:

Curr Biol. 2021 October 11; 31(19): 4314–4326.e5. doi:10.1016/j.cub.2021.07.059.

Transient expression of a GABA receptor subunit during early development is critical for inhibitory synapse maturation and function

Raunak Sinha[1,2,3,*], **William N Grimes**[4,5,#,*], **Julie Wallin**[2,3], **Briana N Ebbinghaus**[2,3], **Kelsey Luu**[6], **Timothy Cherry**[6,7], **Fred Rieke**[4], **Uwe Rudolph**[8,9], **Rachel O Wong**[10], **Mrinalini Hoon**[1,2,3]

[1.]Dept. of Neuroscience, University of Wisconsin-Madison, Madison, WI, USA

[2.]Dept. of Ophthalmology and Visual Sciences, University of Wisconsin-Madison, Madison, WI, USA

[3.]McPherson Eye Research Institute, University of Wisconsin-Madison, Madison, WI, USA

[4.]Dept. of Physiology and Biophysics, University of Washington, Seattle, WA, USA

[5.]National Institute of Neurological Disease and Stroke, NIH, Bethesda, MD, USA

[6.]Center for Developmental Biology and Regenerative Medicine, Seattle Children's Research Institute, Seattle, WA, USA.

[7.]Dept. of Pediatrics, University of Washington-Seattle and the Brotman Baty Institute for Precision Medicine, Seattle, WA, USA

[8.]Dept. of Comparative Biosciences, College of Veterinary Medicine, University of Illinois at Urbana-Champaign, Urbana, IL, USA

[9.]Carl R. Woese Institute for Genomic Biology, University of Illinois at Urbana-Champaign, Urbana, IL, USA

[10.]Dept. of Biological Structure, University of Washington, Seattle, WA, USA

SUMMARY

Developing neural circuits, including GABAergic circuits, switch receptor types. But the role of early GABA receptor expression for establishment of functional inhibitory circuits remains unclear. Tracking the development of GABAergic synapses across axon terminals of retinal

Correspondence should be addressed to Mrinalini Hoon (mhoon@wisc.edu).

[#]present address

[*]these authors contributed equally

AUTHOR CONTRIBUTIONS

M.H. and R.O.W. designed research; R.S., W.N.G., J.W., B.N.E., K.L., T.C., F.R. and M.H. performed research; R.S., W.N.G., J.W., B.N.E., K.L., T.C. and M.H. analyzed data; U.R. contributed new reagents; R.S., R.O.W. and M.H. wrote the paper.

DECLARATION OF INTERESTS

The authors declare no competing interests.

bipolar cells (BCs) we uncovered a crucial role of early $GABA_A$ receptor expression for the formation and function of presynaptic inhibitory synapses. Specifically, early α3-subunit-containing $GABA_A$ ($GABA_A$α3) receptors are a key developmental organizer. Before eye-opening, $GABA_A$α3 gives way to $GABA_A$α1 at individual BC presynaptic inhibitory synapses. The developmental downregulation of $GABA_A$α3 is independent of $GABA_A$α1 expression. Importantly, lack of early $GABA_A$α3 impairs clustering of $GABA_A$α1 and formation of functional $GABA_A$ synapses across mature BC terminals. This impacts the sensitivity of visual responses transmitted through the circuit. Lack of early $GABA_A$α3 also perturbs aggregation of LRRTM4, the organizing protein at GABAergic synapses of rod BC terminals, and their arrangement of output ribbon synapses.

eTOC Blurb

Sinha et al. show that $GABA_A$ synapses on axon terminals of retinal bipolar cells alter receptor types before eye-opening. $GABA_A$α3 receptors present during early development regulate the assembly and function of these synapses by promoting the clustering of $GABA_A$α1 receptors and the organizing protein LRRTM4.

Keywords

inhibitory circuits; synapse formation; GABA receptor; retina; development

INTRODUCTION

Formation of accurate and efficient synapses relies on a collaborative effort of molecular and activity-dependent processes[1]. A common feature of developing neural circuits is a change in pre- and postsynaptic functional properties as circuits mature. For instance, developing inhibitory brainstem circuits switch neurotransmitter types (GABA->Glycine) and developing excitatory NMDA postsynapses switch receptor composition (GluN2B->2A) during maturation[2, 3]. Although these developmental alterations have been documented for brain regions and excitatory and inhibitory neurons across the CNS[2, 4-8], the organizational role of these alterations have been more extensively studied for excitatory than inhibitory circuits.

Inhibitory circuits in the developing CNS are known to switch receptor composition and distinct receptor-types dominate in the immature vs mature CNS[9, 10]. Of note, α3-subunit containing $GABA_A$ receptors ($GABA_A$α3Rs) are widely expressed in the CNS at the time of birth[6, 11, 12], with a much restricted expression in the mature CNS[13-15]. But the role of this early receptor expression for the formation and function of individual inhibitory synapses remains unclear. Here, we focused on presynaptic inhibitory circuits of the mammalian retina to determine the role of early GABA receptors (GABARs) for the formation of functional inhibitory synapses.

Presynaptic inhibition onto axon terminals of neurons is a common circuit-motif that regulates neurotransmitter release. It is found in the spinal motor neuronal circuit[16], the olfactory glomeruli circuit[17] and the mammalian retinal circuit[18]. In the retina, amacrine cell

(AC) interneurons provide presynaptic inhibition onto axon terminals of bipolar cells (BCs) to regulate glutamate release from BCs[19, 20]. This regulation of glutamate release serves several functions, including adjusting the dynamic range of operation of these neurons[21, 22] and regulating the threshold of retinal visual responses[23]. BCs are glutamatergic second-order neurons that relay photoreceptor input from the outer retina to ACs and retinal output neurons (ganglion cells) in the inner retina (Figure 1A). Specific rod and cone BCs transfer dim-light (rod photoreceptor) and bright-light (cone photoreceptor) information to inner retinal neurons. BCs are classified as 'ON' if they depolarize to light increments, or 'OFF' if they depolarize to light decrements[18, 24, 25]. Rod BCs (RBCs) are ON-BCs, whereas cone BCs are either ON or OFF-BCs. BCs receive GABAergic presynaptic inhibition at their terminals, with both $GABA_A$ and $GABA_C$Rs mediating inhibition onto ON-BC boutons[18, 26-29]. Presynaptic inhibition is generated in two ways: (1), an AC receives excitatory input from the same BC that it provides feedback inhibition onto (*reciprocal* connection; Figure 1A'), and (2), an AC receives excitatory input from a different BC (*non-reciprocal* inhibition). Both reciprocal and non-reciprocal synapses can be GABAergic and utilize ionotropic $GABA_A$Rs[30-32], composed of 2α-2β-1γ subunits[33]. In the retina, specific α-subunit (α1-α3) containing $GABA_A$Rs are localized at distinct non-overlapping postsynapses[34, 35].

Here, we determined the role of early $GABA_A$Rs for the developmental organization and function of GABAergic synapses at ON-BC terminals. We chose the mouse retina for our study due to the wide availability of genetic tools that target specific BC and AC-types and retinal $GABA_A$R populations. Combining these genetic tools with electrophysiology, high-resolution light and electron microscopy (EM) we identified a $GABA_A$R rearrangement at developing BC presynaptic inhibitory synapses and uncovered a critical role of early $GABA_A$R expression for the formation of functional presynaptic inhibitory synapses.

RESULTS

Early $GABA_A$α3 receptors are replaced with $GABA_A$α1Rs at retinal BC axon terminals

We first determined which $GABA_A$R-types are expressed at developing BC terminals to identify the receptor-types that provide early presynaptic inhibition. We immunostained for two $GABA_A$R-types in the developing mouse retina: $GABA_A$α3R and $GABA_A$α1R, because these two types have been found at adult BC terminals[26, 28, 36]. In postnatal day 7 (P7) retina, $GABA_A$α3R labeling was abundant at the outer portion of the retinal inner plexiform layer (IPL), where ON-BC axons stratify. $GABA_A$α1R clusters were, however, hardly noticeable in this layer at this early age (Figure 1B). Just before eye-opening, at P12, $GABA_A$α1 clustering increased in this region of the IPL, increasing further by P30. In contrast, $GABA_A$α3R labeling in the ON-lamina of the IPL decreased with age (Figure 1B).

The developmental downregulation of retinal $GABA_A$α3R expression is also reflected in the promoter accessibility of retinal $GABA_A$Rs. Promoter accessibilities of $GABA_A$α3 and $GABA_A$α1 were compared using a previous retinal ATAC-seq (Assay for Transposase-Accessible Chromatin using sequencing) dataset[37] that spanned different time-points (embryonic day 17.5, P0/day of birth, P3-10, P14/eye-opening, and P21). Whole retina analyses showed high promoter accessibility for $GABA_A$Rs at early time-points with

diminished accessibility after eye-opening (Figure S1A). To compare $GABA_A$ promoter accessibility specifically across retinal BCs, we analyzed the Jorstad *et al.*[38] ATAC-seq dataset from adult ON-BCs. This dataset utilized FACS-purified BCs from the adult *Grm6*-tdTomato transgenic line where ON-BCs selectively express the fluorescent protein tdTomato[39]. Comparing $GABA_A\alpha3$ and $GABA_A\alpha1$ promoter accessiblity from adult ON-BCs revealed that whereas the $GABA_A\alpha1$ promoter was still accessible in adult ON-BCs, the $GABA_A\alpha3$ promoter accessiblity was undetectable (Figure S1A). We also compared $GABA_A$ mRNA levels between P6 vs P50 retinas and found an almost 2.5 fold increase in the mRNA levels of $GABA_A\alpha1$ between these time-points, whereas the relative $GABA_A\alpha3$ mRNA levels at P50 reduced to about half their P6 level (Figure S1B).

To visualize $GABA_A\alpha3$ and $GABA_A\alpha1$R clusters specifically on developing BC terminals, we used *Grm6*-tdTomato mice to visualize individual ON-BCs, and immunolabeled these retinas for $GABA_A\alpha3$R and $GABA_A\alpha1$R at different ages (Figure 1C). We focused on two ON-BC types: RBCs that convey dim-light signals and Type 6 ON-cone BCs (T6) that stratify in the same plexus as RBCs but convey high-luminance information. We quantified the percent receptor occupancy of each $GABA_A$R-type relative to axon terminal volume, as a measure of receptor levels. We performed this analysis on P9, P12, P16 and P30 BC terminals (Figure 1C-D). For both RBCs and T6s, $GABA_A\alpha3$ levels were more than 10 fold higher at P9 compared to P30 (RBC P9 $GABA_A\alpha3$= 6.21±0.65; RBC P30 $GABA_A\alpha3$= 0.28±0.07; p-$value_{9vs30}$ = 0.000083: T6 P9 $GABA_A\alpha3$= 5.67±0.16; T6 P30 $GABA_A\alpha3$= 0.48±0.14; p-$value_{9vs30}$ = 0.0075). A rapid decline in $GABA_A\alpha3$R levels was observed around P12 just before eye-opening (Figure 1D). Conversely, axonal $GABA_A\alpha1$R levels of RBCs and T6s increased from P9 until P16 (two days after eye-opening) and thereafter reduced relative to the mature/P30 BC terminal volume (Figure 1D). Together, our observations reveal a developmental downregulation of $GABA_A\alpha3$ with a concomitant increase in $GABA_A\alpha1$ expression during retinal circuit maturation, at both the mRNA and protein level.

To determine whether or not the developmental transition from $GABA_A\alpha3$Rs to $GABA_A\alpha1$Rs on BC axons occurs at the same synapse during maturation, we focused on the A17->RBC GABAergic synapse because of the stereotyped arrangement of this connection across species and the availability of transgenic tools to directly visualize this contact. GABAergic A17 ACs provide reciprocal feedback inhibition onto RBC terminals[23, 40]. Using the Ai9/*slc6a5*-cre double transgenic line in which A17 ACs express tdTomato (Figure S2A), individual A17s were targeted and filled with the dye, lucifer yellow, at two developmental time-points: P11 (before eye-opening) and >P30 (adult/mature). A17 dye-filled retinas were immunolabeled for $GABA_A\alpha3$R or $GABA_A\alpha1$R together with the RBC marker, protein kinase C (PKC)[41], enabling identification of $GABA_A$R-types at A17->RBC synapses (Figure 2A). To quantify $GABA_A$R levels at A17->RBC synapses, the volume overlap between A17 varicosities and RBC terminals (i.e. synaptic contact volume) was digitally isolated, and thereafter the pixel volume of $GABA_A$R immunoreactivity relative to the synaptic overlap volume was expressed as ‘percent occupancy’ (Figure 2B). Before eye-opening (P11), A17->RBC synapses were enriched with $GABA_A\alpha3$Rs. Mature A17->RBC synapses instead largely contained $GABA_A\alpha1$Rs

(Figure 2B), demonstrating a developmental alteration in the $GABA_A$R-type enriched at A17->RBC synapses.

$GABA_A\alpha3$ receptor clustering at BC terminals show a developmental decline even in the absence of $GABA_A\alpha1$

We next determined whether elimination of $GABA_A\alpha1$R from ON-BCs would favor maintenance of high $GABA_A\alpha3$R clusters across adult ON-BC terminals. Crossing the $GABA_A\alpha1$ floxed line[42] with the ON BC-specific *Grm6*-Cre[28] line and the Ai9 reporter line (Ai9/*Grm6*-Cre/$GABA_A\alpha1$ cKO) enabled specific deletion of $GABA_A\alpha1$ from ON BCs ($GABA_A\alpha1$ conditional knockout or cKO) and visualization of the $GABA_A\alpha1$-deficient BCs (Figure S2B). To confirm a lack of $GABA_A$ currents from adult RBCs in the $GABA_A\alpha1$cKO, we performed single-cell patch-clamp recordings from RBCs and recorded their response to GABA-puffs. Previous studies using this technique demonstrated that the GABA-evoked response from RBCs is mediated by both $GABA_C$ and $GABA_A$Rs[19, 28, 36, 43]. We thus measured the RBC response to GABA-puffs at axon terminals before and after application of the $GABA_C$R antagonist, TPMPA (Figure S3A). The difference between these responses, i.e., the $GABA_A$-specific response component, was strikingly lower in $GABA_A\alpha1$cKO RBCs compared to controls (Figure S3A-B), confirming the absence of $GABA_A\alpha1$Rs across adult $GABA_A\alpha1$cKO RBC terminals.

We next analyzed $GABA_A\alpha3$R clustering on adult RBCs and T6s in the $GABA_A\alpha1$cKO. $GABA_A\alpha3$R levels across $GABA_A\alpha1$cKO RBC and T6s were comparable (Figure 3A) to control BCs of the same type. Quantification of $GABA_A\alpha1$R clusters in $GABA_A\alpha1$cKO RBCs and T6s confirmed the downregulation of $GABA_A\alpha1$Rs across both axons and dendrites of KO BCs compared to control (Figure 3B). Quantification of $GABA_A\alpha3$R clusters within $GABA_A\alpha1$cKO RBCs and T6s and control BCs of the same type did not reveal any differences (Figure 3C). Of note, $GABA_A\alpha3$ immunolabeling is restricted to BC axons (Hoon *et al.*[28] and Figure 3C) with negligible $GABA_A\alpha3$R clustering in BC dendrites across genotypes (Figure 3C). Thus, elimination of $GABA_A\alpha1$ from ON-BCs does not alter mature levels of $GABA_A\alpha3$ at BC terminals, underscoring that increasing $GABA_A\alpha1$ expression does not serve as a developmental cue to downregulate $GABA_A\alpha3$ at maturing BC terminals. $GABA_A\alpha3$R levels within $GABA_A\alpha1$cKO RBC terminals were also comparable to controls at P12 (Figure S3C), ruling out compensatory regulation in the $GABA_A\alpha1$cKO early in development, and highlighting a $GABA_A\alpha1$R-independent regulation of $GABA_A\alpha3$R clustering at inhibitory synapses onto ON-BC terminals.

Early presence of $GABA_A\alpha3$ is necessary for accruing $GABA_A\alpha1$Rs at BC terminals

Although $GABA_A\alpha3$R clustering on ON-BCs does not rely on the presence on $GABA_A\alpha1$, the developmental increase in $GABA_A\alpha1$R clusters may depend on the early presence of $GABA_A\alpha3$. To test this hypothesis, we utilized mice that lack expression of $GABA_A\alpha3$ subunits globally[44]. We confirmed that $GABA_A\alpha3$R clustering was abolished in the retinal IPL of the $GABA_A\alpha3$KO (Figure S4A). We next crossed $GABA_A\alpha3$KO mice with *Grm6*-tdTomato mice to enable visualization of individual RBCs and T6s in the KO background. We first quantified the occupancy of $GABA_A\alpha3$ within RBC and T6 terminals in the $GABA_A\alpha3$KO (Figure S4B). $GABA_A\alpha3$ was significantly diminished across terminals of

both BCs in the GABA$_A$α3KO compared to control (Figure S4B). RBC and T6 dendrites showed negligible GABA$_A$α3 clustering across genotypes (Figure S4B).

We next evaluated GABA$_A$α1R clustering in GABA$_A$α3KO retinas (Figure 4). Figure 4A shows a retinal volume of an adult GABA$_A$α3KO and control, immunolabeled for GABA$_A$α1. The outer plexiform layer (OPL) where BC dendrites stratify had comparable GABA$_A$α1 levels across genotypes (Figure 4A). However, the IPL where BC terminals stratify, displayed a striking reduction in GABA$_A$α1 immunolabeling in the GABA$_A$α3KO, compared to control (Figure 4A). The drastic reduction in axonal GABA$_A$α1R clustering was confirmed when we quantified GABA$_A$α1 occupancy at axon terminals of individual RBCs and T6s (Figure 4B-C; GABA$_A$α1 occupancy at BC dendrites was unchanged). Thus, GABA$_A$α1R clustering on RBC and T6 terminals requires the early presence of GABA$_A$α3. GABA$_A$α1R clusters were also significantly downregulated at inhibitory synapses onto another cone BC-type (Type1 OFF cone BC) in the GABA$_A$α3KO (Figure S5A). This BC-type laminates at the opposite border of the IPL and the GABA$_A$α3KO line was crossed to the *Vsx1*-cerulean line[28] to visualize Type1s in the KO. In contrast, glycinergic inhibitory synapses on Type1 terminals, as evaluated by presence of α1-subunit containing glycine receptors at these synapses[28], remained unaltered in the GABA$_A$α3KO (Figure S5B). Thus, the role of early GABA$_A$α3 in establishing GABA$_A$α1R presynaptic inhibitory synapses appears to be conserved across diverse BC-types.

Presynaptic inhibition at RBC and T6 terminals is mediated by both GABA$_A$ and GABA$_C$Rs[28]. Blocking vesicular release of inhibitory neurotransmitters by elimination of the retinal vesicular inhibitory amino acid transporter (VIAAT) impairs maintenance of both GABA$_A$ and GABA$_C$Rs at RBC and T6 terminals[28]. We thus immunolabeled GABA$_C$Rs in GABA$_A$α3KO retina to determine whether or not early expression of GABA$_A$α3 impacts GABA$_C$R clustering at RBC and T6 axons (Figure S6A). GABA$_C$R occupancy remained unperturbed in both RBC and T6 terminals (Figure S6A), suggesting that early GABA$_A$α3 expression specifically regulates maturational changes at GABA$_A$ synapses. GABA$_C$R immunoreactivity on dendrites of RBC and T6s was negligible in both GABA$_A$α3KO and control (Figure S6A), in keeping with previous findings that GABA$_C$R are sparse on ON-BC dendrites[28].

To test whether early GABA$_A$α3 plays a role in the establishment or maintenance of GABA$_A$α1Rs across BC terminals, we quantified GABA$_A$α1R occupancy across P12 GABA$_A$α3KO ON-BC terminals. We observed a substantial reduction of GABA$_A$α1R clustering in P12 GABA$_A$α3KO RBC and T6 terminals relative to control (Figure 4D). Early GABA$_A$α3 expression is thus necessary for the developmental increase of GABA$_A$α1Rs on ON-BC terminals, unlike a lack of VIAAT, which impairs maintenance but not the initial accruing of GABA$_A$α1Rs across RBC and T6 terminals before eye-opening[28]. As an important internal control, GABA$_A$α1R levels across dendrites of the same BCs were not altered in the GABA$_A$α3KO (Figure 4D). We confirmed that GABA$_A$α3 expression was abolished across both axons and dendrites of P12 GABA$_A$α3KO BCs (Figure S4C), and also determined that GABA$_C$R levels at ON-BC axons were unchanged in the P12 GABA$_A$α3KO (Figure S6B). Together, our observations reveal a critical role for GABA$_A$α3 in establishing GABA$_A$α1 inhibitory synapses at developing BC axon terminals.

GABA$_A$Rs do not aggregate at BC axons in GABA$_A$α3KO and failure of GABA$_A$α1 to cluster may be due to impaired receptor trafficking

The lack of GABA$_A$α1R clustering on RBC terminals prompted us to evaluate whether other GABA$_A$R subunits are also affected in the GABA$_A$α3KO. GABA$_A$R pentamers are comprised of 2α-2β-1γ subunits[33], and our previous work has shown that α1-subunits come together with γ2-subunits at GABA$_A$R synapses across ON-BC terminals[28]; see also Wässle *et al.*[34] and Greferath *et al.*[45]. GABA$_A$β2/3 expression is enriched at the outermost lamina of the IPL, where RBC terminals stratify[34, 45, 46] and specifically mRNA for GABA$_A$β3 is found in the layer where BC somata reside[45]. We immunolabeled for GABA$_A$γ2 and GABA$_A$β3-subunits in retinal slices together with the RBC marker, PKC (Figure 5A) and found both receptor subunits to be robustly expressed on wildtype RBC terminals (control panel in Figure 5A). However, in the GABA$_A$α3KO, levels of both GABA$_A$γ2 and GABA$_A$β3-subunits on adult RBC terminals were drastically reduced compared to controls (Figure 5A-B), suggesting a lack of clustering of all GABA$_A$R subunits on adult BC terminals in the absence of early GABA$_A$α3.

Immunolabeling for GABA$_A$α1 reveals the amount of receptor clustered at the postsynaptic surface. Receptor clustering depends not only on total receptor protein expression but also on efficient trafficking from the protein synthesis machinery to the postsynaptic membrane. To determine which of these two possibilities account for decreased GABA$_A$α1R clustering in the GABA$_A$α3KO, we measured the total retinal GABA$_A$α1 protein levels by western blot analyses. Total protein levels of GABA$_A$α1 were equivalent between GABA$_A$α3KO and control retinas (Figure 5C), indicating that GABA$_A$α1 net protein levels are unaltered in the GABA$_A$α3KO. Although we could not measure protein levels specifically in RBCs, the pan-reduction in GABA$_A$α1 clustering in the IPL of the α3KO suggests that it is unlikely that GABA$_A$α1 protein levels were differentially affected across cell-types. We also compared GABA$_A$α1 mRNA levels in GABA$_A$α3KO retinas compared to control and did not observe any change (Figure S6C). As a control, we determined mRNA levels of the RBC specific gene *PCP2*[47] and GABA$_C$ in GABA$_A$α3KO retinas compared to control (Figure S6D). The mRNA levels for both these genes remained comparable across genotypes (Figure S6C-D). As a final assay on the integrity of the GABA$_A$α1 transcriptional machinery in GABA$_A$α3KO retinas, we performed ATAC-seq analyses on adult GABA$_A$α3KO-control retina pairs. We did not observe any noticeable differences in the GABA$_A$α1 promoter accessibility (*Gabra1* locus, Figure 5D) in the GABA$_A$α3KO retina compared to control. Together, our observations suggest that transcription and translation of retinal GABA$_A$α1 is unlikely to be perturbed in the GABA$_A$α3KO, raising the possibility that a deficit in the trafficking of GABA$_A$α1 to the postsynaptic membrane underlies the lack of GABA$_A$α1R clusters on BC axons in the GABA$_A$α3KO.

Lack of GABA$_A$ergic presynaptic inhibition at GABA$_A$α3-deficient rod BC terminals alters rod BC output

To determine how the absence of GABA$_A$α1R clusters in GABA$_A$α3KO retina impacts GABA-evoked currents of RBCs, we performed whole-cell patch-clamp recordings from these BCs in slice preparations of adult retina, and recorded currents in response to GABA-puffs at their axon terminals. GABA-evoked responses in RBCs are mediated by

$GABA_A$ and $GABA_C$Rs[19, 28, 36, 43], with near equal contributions of both receptor-types to the total evoked current amplitude[28, 36, 43]. Comparison of evoked responses of RBCs in $GABA_A$α3KO-control retinas suggests a ~50% reduction in the total GABA-evoked response in the KO (Figure 6A). Application of a $GABA_C$R antagonist (TPMPA) isolated the $GABA_A$-component of the response and revealed that $GABA_A$-mediated currents were substantially reduced in $GABA_A$α3KO RBCs compared to control (Figure 6A). The response remaining in TPMPA was eliminated upon application of the $GABA_A$R antagonist, GABAzine (Figure 6A). The amplitudes of both the total GABA-evoked current and the $GABA_A$R-mediated component were significantly reduced in $GABA_A$α3KO RBCs compared to control (Figure 6B). These recordings corroborate the lack of $GABA_A$R clusters on axon terminals of adult $GABA_A$α3KO RBCs.

A lack of $GABA_A$ inhibition at RBC terminals could affect the efficacy of visual information transfer from RBCs. RBC terminals release glutamate at ribbon synaptic sites apposed to two postsynaptic AC partners. One of the AC partners, the AII, is responsible for conveying visual information from RBCs to ganglion cells[18, 24, 25]. To determine how lack of $GABA_A$ presynaptic inhibition impacts RBC->AII transmission, we performed voltage clamp recordings from AII ACs in $GABA_A$α3KO-control retinas in a wholemount preparation and evaluated responses of AII cells across genotypes. We isolated the excitatory RBC-driven synaptic input across the dim-light regime (Figure 6C). Across flash strengths we observed exaggerated responses from $GABA_A$α3KO AIIs compared to control (Figure 6C). Normalization of the AII response across the flash strengths probed showed a leftward shift of the AII response amplitude vs flash intensity curve in $GABA_A$α3KO compared to control (Figure 6D), indicating an increased light sensitivity of $GABA_A$α3KO AIIs (Figure 6D). We quantified the sensitivity of AIIs across genotypes by fitting the stimulus-response data of individual AIIs with a sigmoid and extracting the flash strength at which the response amplitude reached 50% of its maximum value ($R_{50\%}$). The $R_{50\%}$ value was significantly reduced for $GABA_A$α3KO AIIs compared to control (Figure 6E), confirming an increased light sensitivity of $GABA_A$α3KO AIIs. Our observations thus reveal an abnormal RBC->AII transmission when $GABA_A$ presynaptic inhibition is impaired in the $GABA_A$α3KO.

Synaptic dyad assembly at rod BC terminals is perturbed in the $GABA_A$α3KO

Our observations thus far led us to ask whether clustering of LRRTM4, the organizing protein at GABAergic synapses of RBC axons[43] could also be affected in $GABA_A$α3KOs. We immunolabeled for LRRTM4 in adult $GABA_A$α3KO-control retinas (Figure 7A) and found that LRRTM4 occupancy on RBC terminals was significantly reduced by almost half in $GABA_A$α3KO compared to control (Figure 7B). As GABAergic presynaptic inhibition onto RBC axons is mediated almost equally by $GABA_A$ and $GABA_C$Rs[28, 36, 43], and because $GABA_C$R occupancy is unchanged in the $GABA_A$α3KO (Figure S6A-B), our observations imply that LRRTM4 associated with $GABA_A$ synapses could be selectively altered in $GABA_A$α3KO RBC terminals.

Presynaptic inhibition at RBC terminals regulates assembly of output synapses at these terminals which occur at specialized ribbon sites apposed to two postsynaptic ‘dyad’

partners[43]. Ribbon synapses are sites of glutamate release stereotypically organized such that a single RBC ribbon is apposed to an A17 and AII AC process with the A17 partner providing reciprocal inhibition (Figure 7C). Both loss of inhibitory neurotransmission and LRRTM4 expression were previously found to disrupt the assembly of the RBC dyad, seen as a reduction in the number of ribbons correctly apposed to one AII and one A17 process[43]. We thus performed serial blockface scanning EM and reconstructed RBC terminals in $GABA_A\alpha3$KO retina to determine the ribbon synapse arrangements of adult $GABA_A\alpha3$KO RBC terminals (Figure 7D). On average, we observed 53.67±4.26 ribbons in the $GABA_A\alpha3$KO RBC terminals (n=3) we reconstructed, which was similar to the ribbon numbers in wildtype RBC terminals (50.0±2.08; p-value = 0.48). We then determined the postsynaptic partners at each ribbon site and found several RBC ribbons in the KO erroneously localized across a single AII AC or localized at a three-partner 'triad' junction (Figure 7E-E"); such erroneous contacts were not observed in wildtype. These anomalies led to a significant reduction in the number of $GABA_A\alpha3$KO RBC terminal ribbons correctly apposed across a pair of AII-A17 partners (Figure 7F; correct ribbon assembly rate reduced to 76±3% in the α3KO compared to 91±1% in wildtype). This impairment was less severe than that produced by reduction of both $GABA_A$ and $GABA_C$-mediated inhibition across RBC terminals (e.g. in the LRRTM4KO where the correct dyad assembly is reduced to ~52%[43]). These observations suggest a 'dose-dependent' effect of GABAergic inhibition in influencing RBC dyad assembly. The lack of $GABA_A$-mediated inhibition in $GABA_A\alpha3$KO, however, did not impair the formation of inhibitory synapses across RBC terminals because the number of both reciprocal (A17-mediated) and non-reciprocal inhibitory synapses in the KO was comparable to wildtype (reciprocal synapses at wildtype terminals = 34.00±1.15; reciprocal synapses at $GABA_A\alpha3$KO terminals = 31.33±1.33; p-value = 0.21; nonreciprocal synapses across wildtype terminals = 42.33±1.20; nonreciprocal synapses across $GABA_A\alpha3$KO terminals = 43.00±1.53; p-value = 0.75; n= 3 BCs per genotype).

We also quantified inhibitory synapse number across P12 RBC terminals in $GABA_A\alpha3$KO-control retinas by determining the number of VIAAT-immunoreactive boutons that were spatially apposed to P12 RBC terminals (Figure S6E). We did not observe any difference across genotypes. We verified that the number of inhibitory synapses obtained through our analyses of VIAAT-immunolabeled appositions in wildtype retina (44.13±0.696; n=15 RBC terminals, 7 animals) are comparable to the total number of inhibitory synapses at RBC axonal arbors (reciprocal + non-reciprocal), determined by a serial EM dataset from P12 wildtype retina (45±2; n= 2 RBC terminals reconstructed; P12-EM dataset from Sinha *et al.*[43]). Thus, the total number of inhibitory synapses onto a RBC terminal is not altered in the $GABA_A\alpha3$KO.

DISCUSSION

Role of early GABARs in the development of inhibitory circuits

Our study unveiled an essential role of early $GABA_A\alpha3$ for inhibitory synapse formation and function at axo-axonic synapses. $GABA_A$R clustering was reduced across BC axons in the $GABA_A\alpha3$KO (Figure S7); clustering of several $GABA_A$R subunits, $GABA_A\alpha1$,

GABA$_A$β3 and GABA$_A$γ2, were also diminished. LRRTM4, an organizing protein at GABAergic synapses of RBC axons[43], was also significantly reduced in GABA$_A$α3KOs. These changes are specific to GABA$_A$R synapses; GABA$_C$R synapses adjacent to GABA$_A$R synapses on BC axons[23] were not affected by a loss of GABA$_A$α3. The absence of GABA$_C$ upregulation in GABA$_A$α3KO BCs also underscores a lack of engagement of homeostatic mechanisms to compensate for the loss of GABA$_A$α1 and reduced inhibition. This contrasts with findings in retinas with impaired GABA synthesis where RBCs homeostatically adjust their output[36]. The absence of compensation in GABA$_A$α3KO BC terminals is similar to observations from other brain regions where a loss of GABA$_A$α3 does not cause an upregulation of other GABA$_A$R subunits[48]. Our current observations also suggest that early GABA$_A$α3Rs have a separate role in GABAergic synapse development, distinct from that of inhibitory neurotransmission, which influences clustering of both GABA$_A$ and GABA$_C$Rs at ON-BC terminals[28]. In somatic and dendritic synapses of the thalamic reticular nucleus, GABA$_A$γ2 subunit expression is disrupted in the absence of GABA$_A$α3 and leads to the mis-localization of the inhibitory scaffolding protein, gephyrin, to non-synaptic sites[48]. Thus, early GABA$_A$α3 expression may have common organizational role(s) for inhibitory synapse development at both axons and dendrites and across diverse CNS circuits.

Our estimates of total GABA$_A$α1 protein expression, mRNA levels and promoter accessibility did not yield significant differences between GABA$_A$α3KO-control retinas. The reduced clustering of GABA$_A$α1 at BC axons may therefore be due to perturbed trafficking of GABA$_A$α1 to postsynaptic sites when GABA$_A$α3 is not expressed earlier in development. However, future experiments assessing protein levels specifically from BCs will be needed to test this hypothesis. Whether the physical presence of GABA$_A$α3 is needed to guide GABA$_A$α1 and the scaffolding protein LRRTM4 to GABA$_A$ postsynapses of BC axons, or whether early GABA$_A$α3-mediated transmission is key for recruiting GABA$_A$α1 and LRRTM4 to these synapses is unknown. But our previous observations from retinas deficient in inhibitory neurotransmission (VIAAT or Glutamic acid decarboxylase KO) may help distinguish between these possibilities. We had found that inhibitory neurotransmission regulates the maintenance but not the initial accumulation of GABA$_A$α1Rs on BC terminals[28, 36]. Because GABA$_A$α3 is critical for the initial accruing of GABA$_A$α1Rs at BC axons, it is likely that GABA$_A$α3 regulates the formation of inhibitory synapses onto BC axons through an activity-independent mechanism.

We demonstrate that early GABA$_A$α3Rs are critical for the functional development of GABA$_A$ synapses at RBC terminals. The absence of this receptor-type during development leads to hypersensitivity of AII AC visual responses, and perturbed RBC->AII transmission. The deficiency of GABA$_A$ presynaptic inhibition at GABA$_A$α3KO terminals could underlie the hypersensitivity of AII visual responses. Furthermore, the ultrastructural misarrangements of RBC output ribbon synapses could also contribute towards AIIs receiving abnormal RBC-mediated input. The number of RBC ribbons correctly apposed to an A17-AII pair in the GABA$_A$α3KO was reduced by ~16%. This is, however, not as severe as the disruption to dyad assembly (~37% reduction in AII/A17 dyads) at RBC axons when both GABA$_A$ and GABA$_C$-mediated presynaptic inhibition are impaired[43]. Because GABA$_A$ and GABA$_C$Rs are expressed by RBCs in near equal proportions and contribute equally to the net GABA-evoked responses[28, 36, 43], the extent of error in RBC

dyad assembly may correlate with the 'amount' of presynaptic inhibition onto BC axons during development. Because $GABA_A\alpha3$KO RBCs still have $GABA_C$-mediated inhibition, the ultrastructural mis-arrangements in the assembly of their output synapses may be less severe.

Taken together, our observations underscore a critical role of early $GABA_A\alpha3$ for the formation and function of inhibitory synapses at retinal BC axons. Given the extensive expression of $GABA_A\alpha3$ across developing brain regions, our findings raise the possibility that this receptor-type may have a more widespread developmental role in shaping inhibitory circuits than previously appreciated.

Receptor composition changes at synapses during development

Subunit composition of receptors at the postsynapse is a key determinant of response type and response kinetics. Thus, receptor composition has a direct functional correlate. It is well known that glutamate receptor composition in the CNS changes with circuit maturation. The GluN2B->GluN2A receptor subunit switch results in faster kinetics of NMDA receptor-mediated responses[3]. GluN2A-containing receptors exhibit faster rising and decaying currents compared to GluN2B-containing receptors[3, 7, 49]. The GluN2B->2A switch has also been suggested to support the acquisition or enhancement of learning capabilities[3, 50], with the shift from GluN2B->2A controlling the threshold for modifying synaptic strength[51].

Developing GABAergic neurons have similarly been found to change their GABAR composition to support faster inhibitory responses with maturation. The α–subunit of the $GABA_AR$ is an important determinant of response kinetics[6]. In the thalamic reticular nucleus, $GABA_A\alpha5$-containing receptors mediate prolonged early postnatal tonic inhibitory current and a switch to $GABA_A\alpha3$ allows shortening of inhibitory postsynaptic currents and generation of faster rhythmic oscillations[5]. This receptor-type switch enables facilitation of the spontaneous network activity in the thalamic reticular nucleus, which is important for supporting increased external environment awareness of the organism[5]. $GABA_AR$ subunit changes also occur in the rat visual cortex during development and have been correlated with an accelerated decay of spontaneous inhibitory currents[52]. Like these past findings, our current observations in the retina also reveal a change in the expression of $GABA_A\alpha$ subunits, transitioning from $GABA_A\alpha3$ to $GABA_A\alpha1$, during retinal circuit maturation. However, our findings further demonstrate that such $GABA_A\alpha$-subunit changes at inhibitory synapses occur not only on dendrites of CNS neurons but also on their axons. The decline in $GABA_A\alpha3$ and increase in $GABA_A\alpha1$ at BC axons would ensure faster inhibitory modulation of BC excitatory transmission in the adult. This is because $GABA_A\alpha3$Rs are known to confer inhibition with slower response kinetics compared to $GABA_A\alpha1$Rs[6, 42, 53, 54]. This is likely important for both rod and cone BCs because the $GABA_A\alpha3$->$GABA_A\alpha1$ transition occurs in both BC types. We demonstrate a functional impact when $GABA_A\alpha3$, and thus $GABA_A\alpha1$, are absent in the rod pathway, but the functional consequences of the $GABA_A\alpha3$->$GABA_A\alpha1$ dominance on the cone pathway remains to be determined.

Whether or not the change in $GABA_A\alpha$-subunit expression is also accompanied by modifications of other GABAergic postsynaptic components at BC terminals remains as yet unknown. Developmental alterations in the expression of both receptor subunits and associated scaffolding proteins are known to occur at glutamatergic postsynapses. NMDA receptors switch receptor-types (GluN2B->GluN2A) together with associated scaffolding proteins at a time coincident with synapse maturation[3, 50]. SAP102, a scaffold that forms complexes with GluN2B receptors is replaced with PSD95, a scaffold of GluN2A receptors[3, 55]. We previously found that LRRTM4, a postsynaptic organizing protein, is present at mature RBC $GABA_A\alpha1$ synapses[43]. In the absence of LRRTM4, $GABA_A\alpha1$ accumulation at these synapses is much reduced[43]. In the CNS, LRRTM4 expression is steeply upregulated from the first postnatal week until P30[56] matching the timeline we observe for $GABA_A\alpha1$ expression across RBC terminals. As $GABA_A\alpha3$R clustering on ON-BC terminals is highest around the first postnatal week it is unlikely that LRRTM4 is a common organizing protein of $GABA_A\alpha3$ and $GABA_A\alpha1$-containing BC synapses. Future studies, probably relying on single-BC transcriptomics from early developmental time-points are needed to uncover the identity of organizing protein(s) at early $GABA_A\alpha3$ synapses.

We observed that $GABA_A\alpha3$->$GABA_A\alpha1$R expression transitioned around eye-opening, a correlation that has been observed previously in other CNS regions. The $GABA_A\alpha5$-$GABA_A\alpha3$ switch in thalamic reticular nucleus occurs around the time of eye-opening[5] as does the $GABA_A$R subunit switch in the visual cortex[52]. This common timeline in the expression changes of the α-subunits of $GABA_A$Rs may suggest distinct roles for the early-expressing and late-expressing $GABA_A$R-types in synapse formation versus plasticity. Indeed, in visual cortical circuits, $GABA_A\alpha1$ is pivotal for experience-dependent plasticity but not for circuit development; the reverse is true for $GABA_A\alpha3$Rs[6, 57]. For the retina, however, future experiments are needed to determine whether $GABA_A\alpha1$ and $GABA_A\alpha3$R-types could play distinct roles in supporting plasticity in the inner retina and to uncover the underlying developmental mechanisms regulating the $GABA_A\alpha3$->$GABA_A\alpha1$ dominance at inner retinal synapses.

By examining the stereotypically arranged RBC-A17 synapse, we were able to show that $GABA_A\alpha1$R clustering increases at this synapse during development as $GABA_A\alpha3$ clustering declines. This decline at most RBC-A17 synapses is unlikely to be due to a major loss of early connections, but rather reflects a change in receptor composition at the same synapses. Whether or not receptor subunit composition changes at the same synapse in other parts of the CNS and whether GABAR composition at the mature synapse always depends on the earlier presence of another receptor-type, have yet to be explored in detail. Such studies at the resolution of individual inhibitory synapses would augment our understanding of the process of inhibitory synapse maturation. Our findings here support a mechanism by which already established inhibitory synapses could alter receptor composition during circuit maturation to support functional demands of the emerging circuit.

STAR METHODS

RESOURCE AVAILABILITY

Lead contact—Further information and requests for resources and reagents should be directed to and will be fulfilled by the Lead Contact, Mrinalini Hoon (mhoon@wisc.edu).

Materials availability—This study did not generate any unique reagents.

Data and code availability—The ATAC-seq dataset from $GABA_A\alpha3$KO-littermate control retina has been deposited (GEO: GSE180163). The remaining datasets supporting the current study have not been deposited in a public repository because of extremely large file sizes but are available from the corresponding author on request. This study did not generate a unique code.

EXPERIMENTAL MODELS AND SUBJECT DETAILS

All experiments were performed in accordance with the guidelines of the Institutional Animal Care and Use Committees (IACUC) of the University of Washington and the University of Wisconsin-Madison and the National Institutes of Health. Developing rod BCs and Type 6 ON bipolar cells were visualized in the *Grm6*-tdTomato mouse line[39] in which the metabotropic glutamate receptor-6 (mGluR6) promoter drives tdTomato expression in ON bipolar cells. Age matched littermate control and $GABA_A\alpha3$ KO[44] mice were utilized for analyses. $GABA_A\alpha3$ KO-littermate mice were analyzed at the adult time-point (> 6 weeks) and at P12 (before eye-opening). To visualize rod BCs and Type 6 ON bipolar cells in the $GABA_A\alpha3$ KO, the $GABA_A\alpha3$ KO line was crossed into the *Grm6*-tdTomato background. To visualize Type 1 OFF cone bipolar cells in the $GABA_A\alpha3$ KO, the $GABA_A\alpha3$ KO line was crossed into the *Vsx1*-cerulean mouse line where OFF bipolar cells are specifically labeled by expression of cerulean fluorescent protein[28]. To target A17 amacrine cells, the Ai9 reporter line (Jackson Laboratory, B6.Cg-Gt(ROSA)26Sor$^{tm9(CAG-tdTomato)Hze}$/J) was crossed into the *slc6a5*-cre transgenic (GENSAT) to generate the Ai9/*slc6a5*-cre line. In this line amacrine cells including A17 amacrine cells are fluorescently labeled and can thus be visualized. The Ai9/*slc6a5*-cre line was used to target and fill A17 before eye-opening (P11) and at a mature time point (>P30). To eliminate $GABA_A\alpha1$ receptors from rod BCs ($GABA_A\alpha1$ cKO), the $GABA_A\alpha1$ floxed line (B6.129(FVB)-Gabra1^{tm1Geh}/J) was crossed into the ON bipolar cell specific *Grm6*-Cre[28] line and the Ai9 reporter line. Cre-expressing BCs in a wildtype background served as littermate controls. $GABA_A\alpha1$ cKO-littermate mice were analyzed at the adult time-point (> 6 weeks) and at P12 (before eye-opening). Mice of both sexes were utilized. For gene expression experiments P6 and P50 C57BL6/J wildtype animals (Jackson Laboratory) were utilized. 2 adult C57BL6/J wildtype animals were used in the Control data-set for AII electrophysiological experiments.

METHOD DETAILS

Immunohistochemistry—Immunolabeling was performed on whole-mount retinas isolated in cold oxygenated mouse artificial cerebrospinal fluid (mACSF, pH 7.4) containing (in mM): 119 NaCl, 2.5 KCl, 2.5 CaCl2, 1.3 MgCl2, 1 NaH2PO4, 11 glucose, and 20

HEPES. Retinas were flattened on a filter paper (Millipore, HABG01300), fixed for 15 mins in 4% paraformaldehyde prepared in mACSF, rinsed in phosphate buffer (PBS) and incubated with primary antibody in blocking solution containing 5% donkey serum and 0.5 Triton X-100 at 4°C for 3-4 days. Antibodies utilized were as follows: anti-PKC (1:1000, mouse, Sigma); anti-lucifer yellow (1:500, rabbit, Invitrogen), anti-LRRTM4 (BC-262) (1:500, rabbit[56]); anti-$GABA_A\alpha1$ (1:5000, guinea pig, J.M Fritschy[13]); anti-$GABA_C\rho$ (1:500, rabbit, R. Enz, H. Wassle and S. Haverkamp[34]); anti-$GABA_A\alpha3$ (1:3000, guinea pig, J.M Fritschy[13]), anti-$GABA_A\gamma2$ (1:1000, rabbit, Synaptic Systems), anti-$GABA_A\beta3$ (1:500, guinea pig, Synaptic Systems), anti-GlyR$\alpha1$ (1:500, mouse monoclonal mAb2b, Synaptic Systems), anti-RFP (mouse monoclonal, 1:1000, Abcam), anti-VIAAT (rabbit polyclonal, 1:1000, Synaptic Systems), anti-DsRed (rabbit polyclonal, 1:1000, Clontech). After incubation with primary antibodies, retinas were rinsed in PBS and incubated with anti-isotypic Alexa Fluor (1:1000, Invitrogen) or DyLight (1:1000, Jackson Immunoresearch) secondary antibodies overnight at 4°C. Thereafter retinas were rinsed in PBS and mounted on slides with Vectashield antifade mounting medium (Vector Labs). For generating retina slices, fixed retinas were embedded in agarose (Sigma, low gelling temperature) and sectioned (120 μm) at a Leica Vibratome (VT1000S). The slices were collected in PBS and subsequently processed for immunohistochemistry.

Confocal microscopy and Image analyses—Images were acquired with an Olympus FV 1000 laser scanning confocal microscope and a 1.35 NA 60X oil immersion objective or a Leica SP8 confocal microscope and a 1.4 NA 63X oil immersion objective. Voxel size for acquired images was around 0.05-0.05-0.3 μm (x-y-z). Image stacks were processed using Image J (NIH) and Amira (ThermoFisher Scientific) software. Individual bipolar cell processes were isolated in 3D using the *LabelField* function in Amira. To isolate the receptor signal within a BC process, the receptor channel was multiplied with the BC mask using the *Arithmetic* function in Amira. To quantify the amount of receptor expressed within the BC process, we determined the volume occupied by the receptor signal within the BC terminal and expressed it relative to the volume of the BC terminal (% volume occupancy) as previously described[28, 43, 58]. A threshold was applied to eliminate background pixels and the total volume of receptor signal/pixels above background was thereafter expressed as % occupancy relative to the BC volume[28, 43, 58].

To determine contacts between PKC positive rod BCs and A17 amacrine cell varicosities, the A17 amacrine cell varicosities and rod BC axonal boutons were first masked in 3D using the *LabelField* function in Amira. Using the *Arithmetic* function, the A17 varicosities mask and the rod BC axon terminal mask were then multiplied to determine the synaptic overlap. The GABA receptor channel was thereafter multiplied with the A17- rod BC synaptic overlap channel to isolate the receptor signal specifically within synaptic overlap. % occupancy of receptor signal within the overlap was determined as described above.

To determine appositions of VIAAT-positive terminals (inhibitory presynapses) across PKC positive rod BC boutons, individual rod BC terminals were first masked in 3D (volume isolation) using the *LabelField* function in Amira. Thereafter regions of interest were created for each VIAAT positive puncta that had volume overlap (in 3D) with the rod BC mask.

The number of such VIAAT positive regions of interest were thereafter summed for each complete rod BC terminal.

Electrophysiology recordings and A17 cell fills—Experiments were conducted on dark-adapted $GABA_A\alpha3$ KO and littermate control mice in a whole-mount preparation for AII amacrine cell recording or a slice (200 μm thick) preparation for determining rod BC puff responses from $GABA_A\alpha3$ KO-littermate control mice and $GABA_A\alpha1$ cKO-littermate control mice. For AII recordings 3 littermate control (7 AII cells) and 2 non-littermate wildtype (C57BL6/J) animals (2 AII cells) were used. For recording light responses from AII amacrine cells, isolated retinas were stored in oxygenated (95% O_2/5% CO_2) bicarbonate Ames medium (Sigma) at ~32°C. Retinas were mounted photoreceptor-side down on poly-L-lysine coated cover slips. The mounted retina was continuously super fused with warm oxygenated Ames (~8mL/min). Retinal dissections and mounting were conducted exclusively under infrared illumination (>900nm) to preserve visual sensitivity.

Voltage-clamp whole-cell recordings from AII amacrine cells were conducted with electrodes (5-6 MΩ) containing (in mM): 105 Cs methanesulfonate, 10 TEA-Cl, 20 HEPES, 10 EGTA, 2 QX-314, 5 Mg-ATP, 0.5 Tris-GTP and 0.1 Alexa (594) hydrazide (~280 mOsm; pH ~7.3 with CsOH). To isolate excitatory synaptic input, cells were held at the estimated reversal potential for inhibitory input (−68.5 mV). Absolute voltage values were corrected for liquid junction potentials (−8.5 mV). Full field illumination (diameter: 500-560 μm) was delivered to the photoreceptors through a customized condenser from short wavelength (peak power at 405 or 460 nm) LEDs. Light intensities (photons/μm^2/s) were converted to photoisomerization rates (R*/photoreceptor/s) using the estimated collecting area of rods (0.5 μm^2; Field and Rieke[59], the LED emission spectra and the photoreceptor absorption spectra[60]). Flashes were 10 ms in duration. Electrophysiology example traces in the figures represent the average of ~10 raw responses to the same stimuli. Responses (peak) from individual AII amacrine cells were normalized to the response amplitude at the brightest flash strength (3.2 R*/Rod/flash) and fit with the sigmoid fit function in Igor Pro (Wavemetrics). The flash strength that generates 50% of the maximum AII response amplitude (R_{50}%) was estimated from these fits.

Retinas were embedded in agarose and sliced as previously described[28, 43] for rod BC recordings. For rod BC puff recordings 5 adult $GABA_A\alpha3$ KO animals and 6 littermate control animals were used and 3 adult $GABA_A\alpha1$ cKO and 3 littermate control animals were used. Voltage-clamp recordings from rod BCs used pipettes (10–14 MΩ) filled with an intracellular solution containing (in mM) the following: 105 Cs methanesulfonate, 10 TEA-Cl, 20 HEPES, 10 EGTA, 2 QX-314, 5 Mg-ATP, 0.5 Tris-GTP, and 0.1 Alexa-594 hydrazide (~280 mOsm; pH ~7.2 with KOH). To isolate the $GABA_A$ and $GABA_C$ mediated currents, (1,2,5,6-Tetrahydropyridin-4-yl) methylphosphinic acid (TPMPA, 50 μM; Tocris, Bristol, United Kingdom) and GABAzine (20 μM; Sigma) were added to the perfusion solution. To isolate the GABA mediated inhibitory currents cells were held at the estimated reversal potential for excitatory input ~+10 mV. Absolute voltage values were not corrected for liquid junction potentials (−8.5 mV). GABA was applied using a Picospritzer II (General Valve) connected to a patch pipette (resistance, ~5–7 MΩ). GABA (200 μM) was dissolved in Hepes-buffered Ames medium with 0.1 mM Alexa-488 hydrazide and applied with the

puff pipette. The puffing direction and the duration of the 50 ms puff were selected such that the GABA puff completely covered the axon of the rod BC being recorded from. Our previous studies using this technique have confirmed that the GABA puff application at rod BC axon terminals only activates GABA receptors specifically at the axon terminal[28, 43]. To quantify GABA-evoked currents, peak amplitude was calculated by subtracting the pre-stimulus baseline current from the peak response and averaging across several trials.

A17 cells were targeted with 2-photon microscopy (980 nm) in whole mount retinas[61] from the Ai9/*slc6a5*-cre transgenic line. Two different developmental time points, postnatal day 11 and adult (>4 weeks) were used. A17 cells were injected with 2% Lucifer yellow (LY) prior to fixation with 4% paraformaldehyde (prepared in mACSF) for 15 mins. The retinas were thereafter rinsed with PBS and processed for immunohistochemistry as described above.

3D serial block face serial scanning electron microscopy and rod BC reconstructions—Retinas were immersion fixed in 4% glutaraldehyde in 0.1 M sodium cacodylate buffer (pH 7.4) and were processed and embedded in Durcupan resin as previously described[62]. A Zeiss 3View Serial block face scanning electron microscope was used to image retinal regions comprising a 2x2 montage of tiles (8600x8600 pixels; ~48μmx48μm) at a section thickness of 50nm. Image stacks were aligned, and rod BCs reconstructed using TrakEM2 module of Image J (NIH). Amira (ThermoFisher Scientific) was used for display of reconstructed cell profiles and associated synaptic profiles.

Rod BC terminals were determined in the EM stack by their characteristic morphology[18, 24, 43, 63]. Ribbons at rod BC terminals are apposed to two postsynaptic amacrine interneurons, one of which (the A17) makes a reciprocal feedback inhibitory synapse back onto the same rod BC terminal it receives input from[18, 24, 43, 63]. This feature was used to distinguish A17 profiles at each rod BC ribbon site. The AII partner was recognized through ultrastructural features as previously described[43, 64]. Electron dense ribbons were easily recognized in EM images allowing demarcation of dyad sites and apposed AII and A17 synaptic partners. Inhibitory synapses were determined by the characteristic accumulation of synaptic vesicles along a defined release site and the presence of a thickening of the pre- and postsynaptic membranes as described previously[65]. 3 $GABA_A\alpha3$ KO rod BC terminals were reconstructed from 2 adult animal pairs. A P12 wildtype retina dataset from Sinha *et al.*[43] was used to determine the total inhibitory synapse number across rod P12 BC terminals.

Real Time - Quantitative PCR (qPCR) from retina samples—Retinas were collected from 3 adult $GABA_A\alpha3$ KO and littermate control animals. For the developmental comparison, retinas were collected from 3 P6 and P50 C57BL/6J animal pairs. For each animal, both retinas were pooled into one sample. RNA was extracted using DNA/RNA/Protein extraction kit (IBI Scientific). cDNA was reverse-transcribed using M-MLV reverse transcriptase (Promega) and Oligo(dT) Primers (5′–AAGCAGTGGTATCAACGCAGAGTACT30VN-3)[66]. The same concentration of total RNA was used for each sample. Real-Time qPCRs were run in 10 μL fast reactions (PowerUp SYBR™ Green Master Mix, Applied Biosystems) in a Quant Studio 7

Flex machine (Life Technologies). PCR's were run in pair-matched batches with GAPDH as a reference gene. Relative Gene Expression was calculated using the ΔΔ Ct method with the Pfaffl correction[67]. Primers were used from published literature or designed with the NCBI BLAST tool. New primer pairs were verified by band size and Sanger Sequencing of the PCR product. Product sequences obtained were analyzed with UGENE. Determined primer efficiencies are as follows; GAPDH 1.09, $GABA_A\alpha1$ 0.91, $GABA_A\alpha3$ 0.93, $GABA_C\rho$ 1.05, PCP2 1.03. Primer sequences are as follows: GAPDH[68] Forward: GGCCGGTGCTGAGTATGTCG Reverse: TTCTGGGTGGCAGTGATGGC, $GABA_A\alpha1$ Forward: CACCATGAGGTTGACCGTGA Reverse: CTACAACCACTGAACGGGCT, $GABA_A\alpha3$ Forward: GTGACACTCGATCTCACAGGT Reverse: ATATCTGGGGCATGCTTGGG, $GABA_C\rho$ Forward: GAGTTTCCCTGGGGATCACG Reverse: GCCATGGCTTGAACAGCATC, PCP 2 Forward: CAGACCTTCTAGACAAGGCAGG Reverse: TCGTTTCTGCATTCCATCCTTG.

Assay for Transposase-Accessible Chromatin (ATAC)-Seq analyses—One pair of $GABA_A\alpha3$ KO-littermate control animal was used for the ATAC-Seq experiment. Flash-frozen retinas were thawed by addition of 700μl of lysis buffer (10 mM Tris-HCl, 10 mM NaCl, 3 mM $MgCl_2$, 0.1% NP-40), homogenized by trituration 10x with a p1000 pipet set to 500 μl, dounced in an ice cold RNase-free 2mL glass dounce 10x with a loose pestle and 10x with tight pestle, and transferred back to original 1.5mL LoBind tube (Eppendorf). Dounce was washed with an additional 700μl ice cold lysis buffer and buffer was transferred to tube with sample for a final volume of 1.4mL. Sample was then centrifuged in a microcentrifuge at 4°C for 10min at 500 rcf. The pellet was re-eluted in 1.4mL ice cold lysis buffer, transferred to a pre-chilled dounce, homogenized again 12x with tight pestle, and transferred back to 1.5mL LoBind tube. Nuclei were counted on a hemocytometer and the volume of lysis buffer/nuclei suspension needed for 20,000 nuclei was aliquoted into a separate 1.5mL LoBind tube. Samples were centrifuged along with tube containing remaining nuclei (for nuclear localized RNA) at 4°C for 5 min at 500g (RCF). The supernatant was removed from samples and remaining nuclei. Subsequent ATAC libraries were generated with 20,000 nuclei per sample using the Nextera DNA library prep kit (FC-121-1030; Illumina, San Diego, CA USA) according to the protocol described in Buenrostro *et al.*[69, 70]. ATAC-Seq libraries were prepared and sequenced on the Illumina NextSeq 500 platform with 75 bp single-end reads.

For ATAC-Seq Read processing and alignment. Demultiplexed FASTQ files were trimmed with Trimmomatic (version 0.33) using the parameter SLIDINGWINDOW:5:30[71]. Trimmed reads were indexed and aligned to the mouse genome (Mouse GRCm38/mm10 assembly, December 2011) using the Burrows-Wheeler Aligner (bwa) tool[72] with the parameters: bwa aln -q 0 -t 4 -n 2 -k 2 -l 32 -e −1 -o 0 and bwa samse -n 5. Tag directories of reads were created using HOMER (version 4.6) makeTagDirectory[73]. Bed files from processed and aligned sequence reads were extended to 200bp and normalized to 10M reads using BEDtools (version 2.23.0)[74] genomeCoverageBED using the -scale parameter before being converted into bigWig format for display on the UCSC genome browser (https://genome.ucsc.edu/).

Western Blot—Retinae from $GABA_A\alpha3$ KO and littermate control mice were homogenized in lysis buffer containing 50mM Tris, 100mM NaCl, 1% Triton X-100, 5mM EDTA, 0.1% SDS, 2.5% glycerol and 1x protease inhibitor cocktail. Both retinas were pooled per animal. Equal amounts of protein samples were run in a 10% SDS gel (Bio-Rad Labs), blotted onto nitrocellulose membranes, incubated with antibodies and visualized by ECL. Primary antibodies utilized were anti-$GABA_A\alpha1$ (clone N95/35 from NeuroMab at 1:5000) and anti-Actin (mouse monoclonal 1:5000 Chemicon).

QUANTIFICATION AND STATISTICAL ANALYSIS

Statistical details of experiments including number of cells (denoted as n) and number of animals (denoted as N) analyzed is provided in the Figure legends. All data are presented as mean ± SEM (standard error of mean) and an unpaired two-tailed T-test was used to determine significance across genotypes.

Supplementary Material

Refer to Web version on PubMed Central for supplementary material.

ACKNOWLEDGEMENTS

This work was supported by NIH Grants EY031677 (to M.H.), EY10699 (to R.O.W.), EY026070 (to R.S.), EY028111 (to F.R.), Vision Core Grant EY01730 (to M. Neitz), Core grant for Vision Research (P30EY016665), the McPherson Eye Research Institute's Rebecca Meyer Brown/Retina Research Foundation Professorship (to M.H), and an unrestricted Grant from Research to Prevent Blindness, Inc. to UW Madison Department of Ophthalmology. We thank J.M. Fritschy, R. Enz, S. Haverkamp and H. Wässle for generously providing $GABA_A$ and $GABA_C$ receptor antibodies, T.J. Siddiqui for generously providing the LRRTM4 antibody and E. Parker, M. Zhang and K. Oda for expert technical assistance.

REFERENCES

1. Sudhof TC (2018). Towards an Understanding of Synapse Formation. Neuron 100, 276–293. [PubMed: 30359597]
2. Gamlin CR, Yu WQ, Wong ROL, and Hoon M (2018). Assembly and maintenance of GABAergic and Glycinergic circuits in the mammalian nervous system. Neural Dev 13, 12. [PubMed: 29875009]
3. Paoletti P, Bellone C, and Zhou Q (2013). NMDA receptor subunit diversity: impact on receptor properties, synaptic plasticity and disease. Nat Rev Neurosci 14, 383–400. [PubMed: 23686171]
4. Lohmann C, and Kessels HW (2014). The developmental stages of synaptic plasticity. J Physiol 592, 13–31. [PubMed: 24144877]
5. Pangratz-Fuehrer S, Sieghart W, Rudolph U, Parada I, and Huguenard JR (2016). Early postnatal switch in GABAA receptor alpha-subunits in the reticular thalamic nucleus. J Neurophysiol 115, 1183–1195. [PubMed: 26631150]
6. Bosman LW, Rosahl TW, and Brussaard AB (2002). Neonatal development of the rat visual cortex: synaptic function of GABAA receptor alpha subunits. J Physiol 545, 169–181. [PubMed: 12433958]
7. Flint AC, Maisch US, Weishaupt JH, Kriegstein AR, and Monyer H (1997). NR2A subunit expression shortens NMDA receptor synaptic currents in developing neocortex. J Neurosci 17, 2469–2476. [PubMed: 9065507]
8. Sheng M, Cummings J, Roldan LA, Jan YN, and Jan LY (1994). Changing subunit composition of heteromeric NMDA receptors during development of rat cortex. Nature 368, 144–147. [PubMed: 8139656]

9. Malosio ML, Marqueze-Pouey B, Kuhse J, and Betz H (1991). Widespread expression of glycine receptor subunit mRNAs in the adult and developing rat brain. EMBO J 10, 2401–2409. [PubMed: 1651228]
10. Fritschy JM, Paysan J, Enna A, and Mohler H (1994). Switch in the expression of rat GABAA-receptor subtypes during postnatal development: an immunohistochemical study. J Neurosci 14, 5302–5324. [PubMed: 8083738]
11. Laurie DJ, Wisden W, and Seeburg PH (1992). The distribution of thirteen GABAA receptor subunit mRNAs in the rat brain. III. Embryonic and postnatal development. J Neurosci 12, 4151–4172. [PubMed: 1331359]
12. Liu Q, and Wong-Riley MT (2004). Developmental changes in the expression of GABAA receptor subunits alpha1, alpha2, and alpha3 in the rat pre-Botzinger complex. J Appl Physiol (1985) 96, 1825–1831. [PubMed: 14729731]
13. Fritschy JM, and Mohler H (1995). GABAA-receptor heterogeneity in the adult rat brain: differential regional and cellular distribution of seven major subunits. J Comp Neurol 359, 154–194. [PubMed: 8557845]
14. McKernan RM, and Whiting PJ (1996). Which GABAA-receptor subtypes really occur in the brain? Trends Neurosci 19, 139–143. [PubMed: 8658597]
15. Pirker S, Schwarzer C, Wieselthaler A, Sieghart W, and Sperk G (2000). GABA(A) receptors: immunocytochemical distribution of 13 subunits in the adult rat brain. Neuroscience 101, 815–850. [PubMed: 11113332]
16. Fink AJ, Croce KR, Huang ZJ, Abbott LF, Jessell TM, and Azim E (2014). Presynaptic inhibition of spinal sensory feedback ensures smooth movement. Nature 509, 43–48. [PubMed: 24784215]
17. McGann JP (2013). Presynaptic inhibition of olfactory sensory neurons: new mechanisms and potential functions. Chem Senses 38, 459–474. [PubMed: 23761680]
18. Hoon M, Okawa H, Della Santina L, and Wong RO (2014). Functional architecture of the retina: development and disease. Prog Retin Eye Res 42, 44–84. [PubMed: 24984227]
19. Eggers ED, McCall MA, and Lukasiewicz PD (2007). Presynaptic inhibition differentially shapes transmission in distinct circuits in the mouse retina. J Physiol 582, 569–582. [PubMed: 17463042]
20. Eggers ED, and Lukasiewicz PD (2011). Multiple pathways of inhibition shape bipolar cell responses in the retina. Vis Neurosci 28, 95–108. [PubMed: 20932357]
21. Sagdullaev BT, McCall MA, and Lukasiewicz PD (2006). Presynaptic inhibition modulates spillover, creating distinct dynamic response ranges of sensory output. Neuron 50, 923–935. [PubMed: 16772173]
22. Pan F, Toychiev A, Zhang Y, Atlasz T, Ramakrishnan H, Roy K, Volgyi B, Akopian A, and Bloomfield SA (2016). Inhibitory masking controls the threshold sensitivity of retinal ganglion cells. J Physiol 594, 6679–6699. [PubMed: 27350405]
23. Grimes WN, Zhang J, Tian H, Graydon CW, Hoon M, Rieke F, and Diamond JS (2015). Complex inhibitory microcircuitry regulates retinal signaling near visual threshold. J Neurophysiol 114, 341–353. [PubMed: 25972578]
24. Wassle H (2004). Parallel processing in the mammalian retina. Nat Rev Neurosci 5, 747–757. [PubMed: 15378035]
25. Demb JB, and Singer JH (2015). Functional Circuitry of the Retina. Annu Rev Vis Sci 1, 263–289. [PubMed: 28532365]
26. Fletcher EL, Koulen P, and Wassle H (1998). GABAA and GABAC receptors on mammalian rod bipolar cells. J Comp Neurol 396, 351–365. [PubMed: 9624589]
27. Koulen P, Brandstatter JH, Enz R, Bormann J, and Wassle H (1998). Synaptic clustering of GABA(C) receptor rho-subunits in the rat retina. Eur J Neurosci 10, 115–127. [PubMed: 9753119]
28. Hoon M, Sinha R, Okawa H, Suzuki SC, Hirano AA, Brecha N, Rieke F, and Wong RO (2015). Neurotransmission plays contrasting roles in the maturation of inhibitory synapses on axons and dendrites of retinal bipolar cells. Proc Natl Acad Sci U S A 112, 12840–12845. [PubMed: 26420868]
29. Eggers ED, and Lukasiewicz PD (2006). GABA(A), GABA(C) and glycine receptor-mediated inhibition differentially affects light-evoked signalling from mouse retinal rod bipolar cells. J Physiol 572, 215–225. [PubMed: 16439422]

30. Singer JH, and Diamond JS (2003). Sustained Ca2+ entry elicits transient postsynaptic currents at a retinal ribbon synapse. J Neurosci 23, 10923–10933. [PubMed: 14645488]
31. Chavez AE, Singer JH, and Diamond JS (2006). Fast neurotransmitter release triggered by Ca influx through AMPA-type glutamate receptors. Nature 443, 705–708. [PubMed: 17036006]
32. Chavez AE, Grimes WN, and Diamond JS (2010). Mechanisms underlying lateral GABAergic feedback onto rod bipolar cells in rat retina. J Neurosci 30, 2330–2339. [PubMed: 20147559]
33. Moss SJ, and Smart TG (2001). Constructing inhibitory synapses. Nat Rev Neurosci 2, 240–250. [PubMed: 11283747]
34. Wassle H, Koulen P, Brandstatter JH, Fletcher EL, and Becker CM (1998). Glycine and GABA receptors in the mammalian retina. Vision Res 38, 1411–1430. [PubMed: 9667008]
35. Koulen P, Sassoe-Pognetto M, Grunert U, and Wassle H (1996). Selective clustering of GABA(A) and glycine receptors in the mammalian retina. J Neurosci 16, 2127–2140. [PubMed: 8604056]
36. Schubert T, Hoon M, Euler T, Lukasiewicz PD, and Wong RO (2013). Developmental regulation and activity-dependent maintenance of GABAergic presynaptic inhibition onto rod bipolar cell axonal terminals. Neuron 78, 124–137. [PubMed: 23583111]
37. Aldiri I, Xu B, Wang L, Chen X, Hiler D, Griffiths L, Valentine M, Shirinifard A, Thiagarajan S, Sablauer A, et al. (2017). The Dynamic Epigenetic Landscape of the Retina During Development, Reprogramming, and Tumorigenesis. Neuron 94, 550–568 e510. [PubMed: 28472656]
38. Jorstad NL, Wilken MS, Grimes WN, Wohl SG, VandenBosch LS, Yoshimatsu T, Wong RO, Rieke F, and Reh TA (2017). Stimulation of functional neuronal regeneration from Muller glia in adult mice. Nature 548, 103–107. [PubMed: 28746305]
39. Kerschensteiner D, Morgan JL, Parker ED, Lewis RM, and Wong RO (2009). Neurotransmission selectively regulates synapse formation in parallel circuits in vivo. Nature 460, 1016–1020. [PubMed: 19693082]
40. Grimes WN, Zhang J, Graydon CW, Kachar B, and Diamond JS (2010). Retinal parallel processors: more than 100 independent microcircuits operate within a single interneuron. Neuron 65, 873–885. [PubMed: 20346762]
41. Haverkamp S, and Wassle H (2000). Immunocytochemical analysis of the mouse retina. J Comp Neurol 424, 1–23. [PubMed: 10888735]
42. Vicini S, Ferguson C, Prybylowski K, Kralic J, Morrow AL, and Homanics GE (2001). GABA(A) receptor alpha1 subunit deletion prevents developmental changes of inhibitory synaptic currents in cerebellar neurons. J Neurosci 21, 3009–3016. [PubMed: 11312285]
43. Sinha R, Siddiqui TJ, Padmanabhan N, Wallin J, Zhang C, Karimi B, Rieke F, Craig AM, Wong RO, and Hoon M (2020). LRRTM4: A Novel Regulator of Presynaptic Inhibition and Ribbon Synapse Arrangements of Retinal Bipolar Cells. Neuron 105, 1007–1017 e1005. [PubMed: 31974009]
44. Yee BK, Keist R, von Boehmer L, Studer R, Benke D, Hagenbuch N, Dong Y, Malenka RC, Fritschy JM, Bluethmann H, et al. (2005). A schizophrenia-related sensorimotor deficit links alpha 3-containing GABAA receptors to a dopamine hyperfunction. Proc Natl Acad Sci U S A 102, 17154–17159. [PubMed: 16284244]
45. Greferath U, Grunert U, Fritschy JM, Stephenson A, Mohler H, and Wassle H (1995). GABAA receptor subunits have differential distributions in the rat retina: in situ hybridization and immunohistochemistry. J Comp Neurol 353, 553–571. [PubMed: 7759615]
46. Greferath U, Muller F, Wassle H, Shivers B, and Seeburg P (1993). Localization of GABAA receptors in the rat retina. Vis Neurosci 10, 551–561. [PubMed: 8388246]
47. Woods SM, Mountjoy E, Muir D, Ross SE, and Atan D (2018). A comparative analysis of rod bipolar cell transcriptomes identifies novel genes implicated in night vision. Sci Rep 8, 5506. [PubMed: 29615777]
48. Studer R, von Boehmer L, Haenggi T, Schweizer C, Benke D, Rudolph U, and Fritschy JM (2006). Alteration of GABAergic synapses and gephyrin clusters in the thalamic reticular nucleus of GABAA receptor alpha3 subunit-null mice. Eur J Neurosci 24, 1307–1315. [PubMed: 16987218]
49. Vicini S, Wang JF, Li JH, Zhu WJ, Wang YH, Luo JH, Wolfe BB, and Grayson DR (1998). Functional and pharmacological differences between recombinant N-methyl-D-aspartate receptors. J Neurophysiol 79, 555–566. [PubMed: 9463421]

50. Dumas TC (2005). Developmental regulation of cognitive abilities: modified composition of a molecular switch turns on associative learning. Prog Neurobiol 76, 189–211. [PubMed: 16181726]
51. Yashiro K, and Philpot BD (2008). Regulation of NMDA receptor subunit expression and its implications for LTD, LTP, and metaplasticity. Neuropharmacology 55, 1081–1094. [PubMed: 18755202]
52. Heinen K, Bosman LW, Spijker S, van Pelt J, Smit AB, Voorn P, Baker RE, and Brussaard AB (2004). GABAA receptor maturation in relation to eye opening in the rat visual cortex. Neuroscience 124, 161–171. [PubMed: 14960348]
53. Gingrich KJ, Roberts WA, and Kass RS (1995). Dependence of the GABAA receptor gating kinetics on the alpha-subunit isoform: implications for structure-function relations and synaptic transmission. J Physiol 489 (Pt 2), 529–543. [PubMed: 8847645]
54. Barberis A, Mozrzymas JW, Ortinski PI, and Vicini S (2007). Desensitization and binding properties determine distinct alpha1beta2gamma2 and alpha3beta2gamma2 GABA(A) receptor-channel kinetic behavior. Eur J Neurosci 25, 2726–2740. [PubMed: 17561840]
55. Sans N, Petralia RS, Wang YX, Blahos J 2nd, Hell JW, and Wenthold RJ (2000). A developmental change in NMDA receptor-associated proteins at hippocampal synapses. J Neurosci 20, 1260–1271. [PubMed: 10648730]
56. Siddiqui TJ, Tari PK, Connor SA, Zhang P, Dobie FA, She K, Kawabe H, Wang YT, Brose N, and Craig AM (2013). An LRRTM4-HSPG complex mediates excitatory synapse development on dentate gyrus granule cells. Neuron 79, 680–695. [PubMed: 23911104]
57. Fagiolini M, Fritschy JM, Low K, Mohler H, Rudolph U, and Hensch TK (2004). Specific GABAA circuits for visual cortical plasticity. Science 303, 1681–1683. [PubMed: 15017002]
58. Hoon M, Sinha R, and Okawa H (2017). Using Fluorescent Markers to Estimate Synaptic Connectivity In Situ. Methods Mol Biol 1538, 293–320. [PubMed: 27943198]
59. Field GD, and Rieke F (2002). Nonlinear signal transfer from mouse rods to bipolar cells and implications for visual sensitivity. Neuron 34, 773–785. [PubMed: 12062023]
60. Govardovskii VI, Fyhrquist N, Reuter T, Kuzmin DG, and Donner K (2000). In search of the visual pigment template. Vis Neurosci 17, 509–528. [PubMed: 11016572]
61. Grimes WN, Hoon M, Briggman KL, Wong RO, and Rieke F (2014). Cross-synaptic synchrony and transmission of signal and noise across the mouse retina. Elife 3, e03892. [PubMed: 25180102]
62. Della Santina L, Kuo SP, Yoshimatsu T, Okawa H, Suzuki SC, Hoon M, Tsuboyama K, Rieke F, and Wong ROL (2016). Glutamatergic Monopolar Interneurons Provide a Novel Pathway of Excitation in the Mouse Retina. Curr Biol 26, 2070–2077. [PubMed: 27426514]
63. Tsukamoto Y, and Omi N (2017). Classification of Mouse Retinal Bipolar Cells: Type-Specific Connectivity with Special Reference to Rod-Driven AII Amacrine Pathways. Front Neuroanat 11, 92. [PubMed: 29114208]
64. Gamlin CR, Zhang C, Dyer MA, and Wong ROL (2020). Distinct Developmental Mechanisms Act Independently to Shape Biased Synaptic Divergence from an Inhibitory Neuron. Curr Biol 30, 1258–1268 e1252. [PubMed: 32109390]
65. Gray EG (1969). Electron microscopy of excitatory and inhibitory synapses: a brief review. Prog Brain Res 31, 141–155. [PubMed: 4899407]
66. Picelli S, Faridani OR, Bjorklund AK, Winberg G, Sagasser S, and Sandberg R (2014). Full-length RNA-seq from single cells using Smart-seq2. Nat Protoc 9, 171–181. [PubMed: 24385147]
67. Pfaffl MW (2001). A new mathematical model for relative quantification in real-time RT-PCR. Nucleic Acids Res 29, e45. [PubMed: 11328886]
68. Nickells RW, and Pelzel HR (2015). Tools and resources for analyzing gene expression changes in glaucomatous neurodegeneration. Exp Eye Res 141, 99–110. [PubMed: 25999234]
69. Buenrostro JD, Giresi PG, Zaba LC, Chang HY, and Greenleaf WJ (2013). Transposition of native chromatin for fast and sensitive epigenomic profiling of open chromatin, DNA-binding proteins and nucleosome position. Nat Methods 10, 1213–1218. [PubMed: 24097267]
70. Buenrostro JD, Wu B, Chang HY, and Greenleaf WJ (2015). ATAC-seq: A Method for Assaying Chromatin Accessibility Genome-Wide. Curr Protoc Mol Biol 109, 21 29 21–21 29 29.

71. Bolger AM, Lohse M, and Usadel B (2014). Trimmomatic: a flexible trimmer for Illumina sequence data. Bioinformatics 30, 2114–2120. [PubMed: 24695404]

72. Li H, and Durbin R (2010). Fast and accurate long-read alignment with Burrows-Wheeler transform. Bioinformatics 26, 589–595. [PubMed: 20080505]

73. Heinz S, Benner C, Spann N, Bertolino E, Lin YC, Laslo P, Cheng JX, Murre C, Singh H, and Glass CK (2010). Simple combinations of lineage-determining transcription factors prime cis-regulatory elements required for macrophage and B cell identities. Mol Cell 38, 576–589. [PubMed: 20513432]

74. Quinlan AR, and Hall IM (2010). BEDTools: a flexible suite of utilities for comparing genomic features. Bioinformatics 26, 841–842. [PubMed: 20110278]

HIGHLIGHTS

1. $GABA_A$ synapses on bipolar cell axons change receptor types before eye-opening.
2. $GABA_A\alpha3$ recruits $GABA_A\alpha1$ and LRRTM4 to inhibitory synapses on bipolar cell axons.
3. Early $GABA_A\alpha3$ is required for functional $GABA_A$ synapses on mature bipolar cell axons.
4. Early $GABA_A\alpha3$ expression regulates organization of rod bipolar cell ribbon synapses.

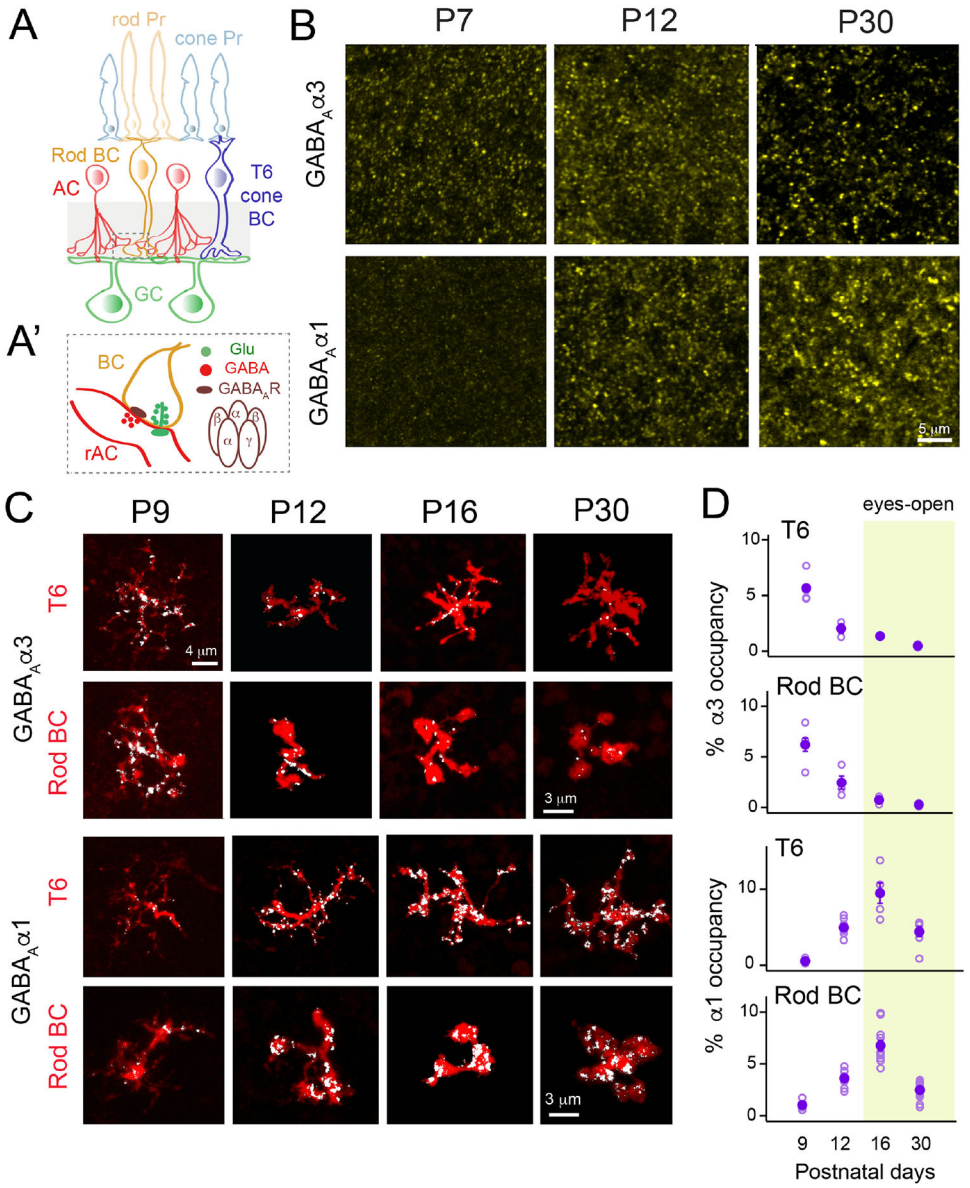

Figure 1: Retinal BC terminals replace GABA$_A$α3 for GABA$_A$α1 during development.

(A) Schematic of the vertebrate retina, showing rod and cone photoreceptors (Pr) providing input to rod and cone bipolar cells (BCs). Cone BCs transfer visual signals to output ganglion cells (GC). BC terminals receive inhibitory input from amacrine cells (ACs) at the inner plexiform layer (IPL) of the retina (shaded grey box).

(A') Glutamate (Glu) release at BC ribbon synapses is modulated by presynaptic inhibition from ACs. Enlarged view of a reciprocal GABAergic AC (rAC) which receives BC input and provides feedback inhibition, mediated by pentameric GABA$_A$Rs composed of α, β and γ subunits.

(B) Single confocal image planes at the level of the IPL where rod BC axons stratify, co-labeled for GABA$_A$α3 and GABA$_A$α1Rs across development (P:postnatal day).

(C) Expression of GABA$_A$α3 and GABA$_A$α1Rs (pixels above background shown in white) within terminals (red) of developing rod and T6 BCs.

(D) % $GABA_A\alpha3$ and $GABA_A\alpha1$ occupancy within developing BC axons. For each time-point n>4 cells and N>3 animals; $GABA_A\alpha1$ P12-P30 data from Hoon *et al.*[28]. Data plotted as mean±SEM for all Figures.
See also Figure S1 and S7.

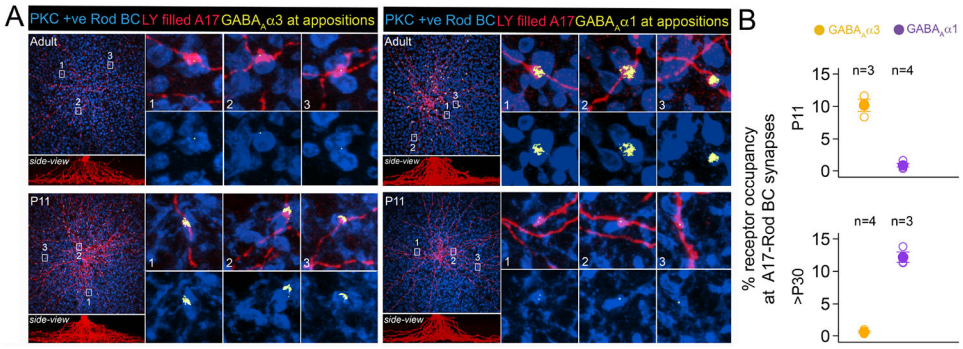

Figure 2: Individual A17-rod BC inhibitory synapses alter their GABA$_A$R-type before eye-opening.

(A) Top-down view of lucifer yellow (LY/red) filled A17s in adult and P11 retinas co-immunolabeled with PKC (blue) and GABA$_A$α3 or GABA$_A$α1Rs (yellow). The GABA$_A$ signal above background and within the A17-RBC volume-overlap is depicted in yellow pixels. Higher-magnification views of three regions per A17, and side-view of the A17-fills are provided.

(B) % GABA$_A$ occupancy at A17-rod BC appositions in P11 (*top*) and mature retina (>P30; *bottom* plot). n=number of A17s analyzed. Each retina-piece contained a single A17-fill; N=3 animals.

See also Figure S2 and S7.

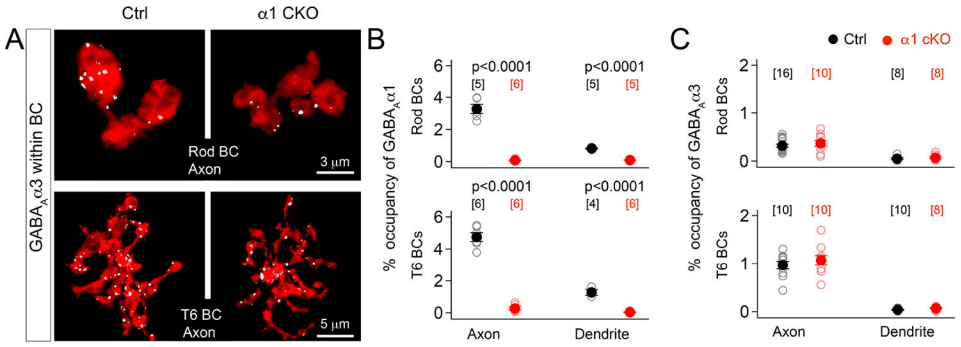

Figure 3: Absence of GABA$_A$α1 on BC axons does not impact GABA$_A$α3R clustering within adult terminals.

(A) Examples of GABA$_A$α3 signal (white pixels represent signal above background) within adult rod BC (*top*) and T6 (*bottom* panel: red) terminals in GABA$_A$α1cKO-littermate control (Ctrl) retina.

% occupancy of GABA$_A$α1 **(B)** and of GABA$_A$α3 **(C)** within adult α1cKO-Ctrl BC axons and dendrites (*top* plots: rod BC; bottom plots:T6). N≥4 GABA$_A$α1 cKO-Ctrl pairs. For all Figures: Number in parenthesis indicates cells analyzed and p-value listed for two-tailed unpaired T-test.

See also Figure S2-3 and S7.

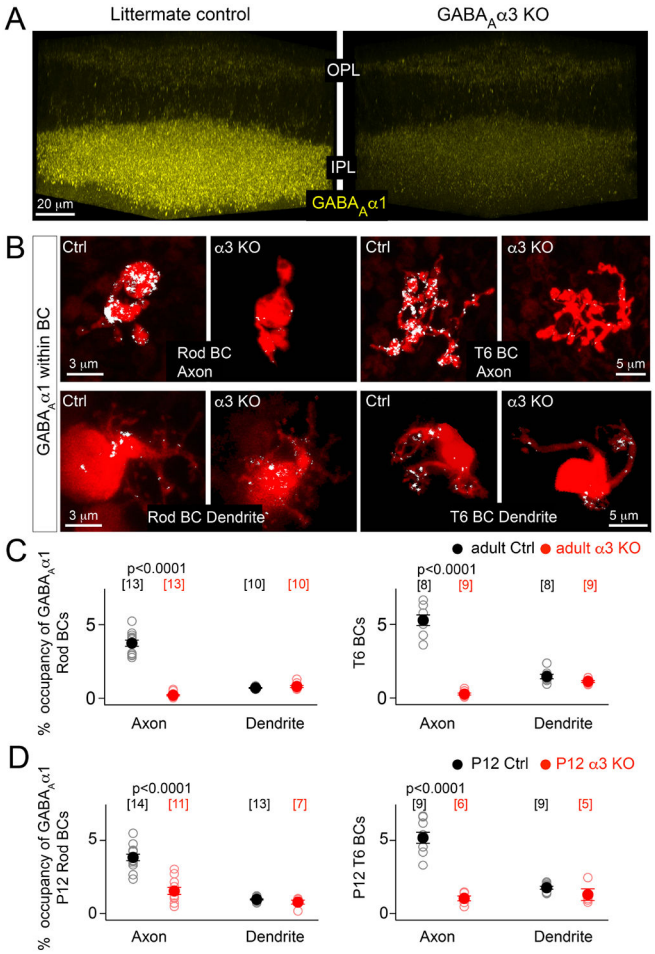

Figure 4: GABA$_A$α1R clustering across BC terminals requires early GABA$_A$α3 expression.

(A) Volume views of GABA$_A$α1 immunofluorescence in the outer and inner plexiform layers (OPL; IPL) of an adult GABA$_A$α3KO and littermate control retina.

(B) GABA$_A$α1 expression (white pixels) within adult rod (*left*) and T6 (*right*) BC axons and dendrites in GABA$_A$α3KO-littermate control (Ctrl) retina.

(C) % GABA$_A$α1 occupancy within adult GABA$_A$α3KO-Ctrl BC axons and dendrites (*left*: rod BC; *right* plot:T6). N>5 GABA$_A$α3KO-Ctrl pairs.

(D) % occupancy of GABA$_A$α1 within P12 GABA$_A$α3KO-Ctrl BC axons and dendrites (*left*: rod BC; *right* plot:T6). N>4 GABA$_A$α3KO-Ctrl pairs.

See also Figures S4-7.

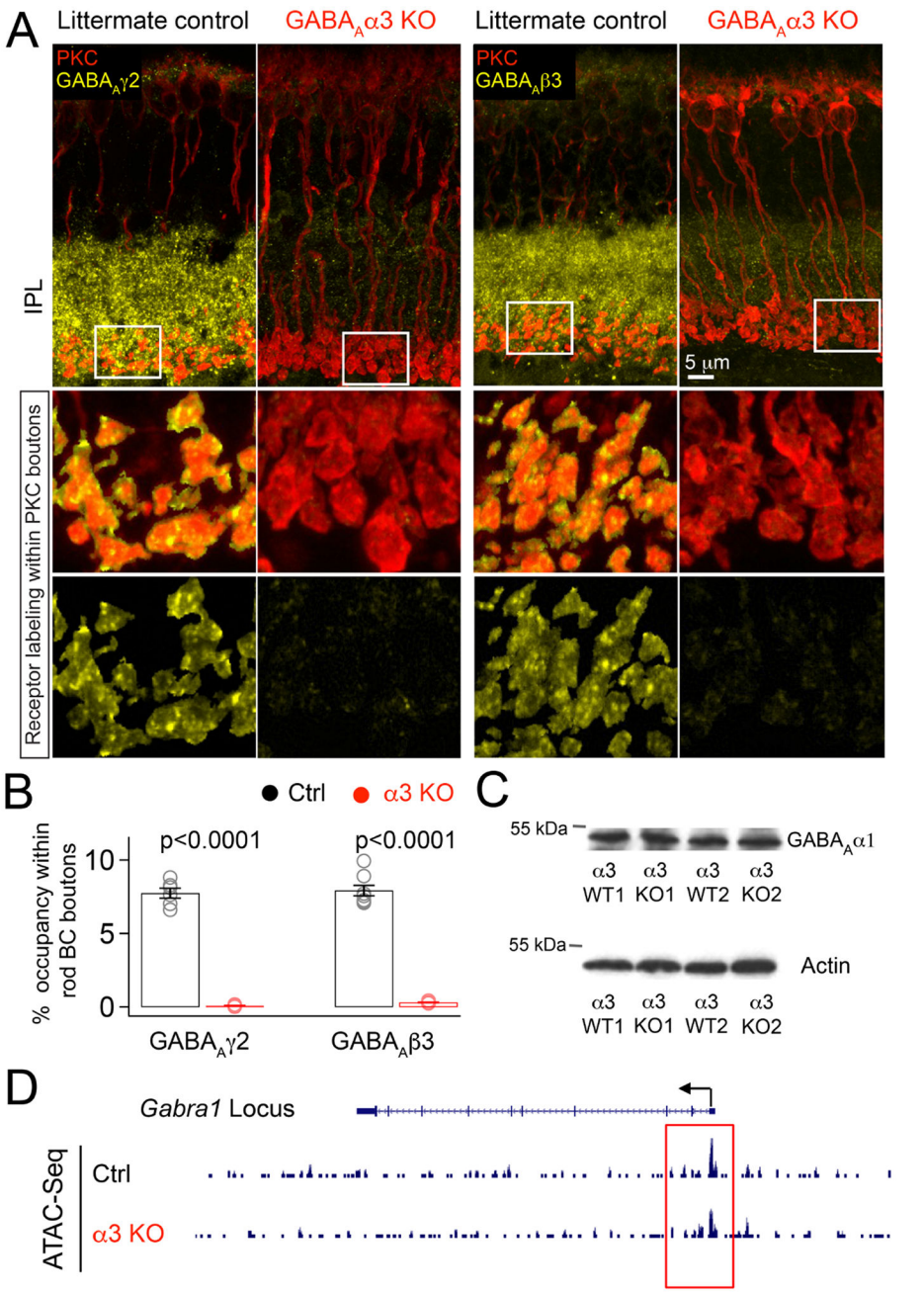

Figure 5: GABA$_A$R subunits are downregulated in GABA$_A$α3KO but GABA$_A$α1 total protein expression and promoter accessibility are unchanged in α3KO retina.

(A) Slices from adult GABA$_A$α3KO-littermate control retinas co-immunolabeled for PKC (red) and GABA$_A$γ2 (*left*) or GABA$_A$β3 (*right* panel: yellow). Bottom panels show higher-magnification views of the selected regions (white box) showing receptor immunostaining within PKC-labeled boutons.

(B) % occupancy of GABA$_A$γ2 and GABA$_A$β3 within adult rod BC boutons across genotypes (N>4 GABA$_A$α3KO-Ctrl pairs; ≥6 sections analyzed per condition).

(C) Western blot showing total protein levels of $GABA_A\alpha1$ compared to the reference Actin, of retinas from two pairs of adult $GABA_A\alpha3$KO-littermate control animals (KO-WT respectively).

(D) Normalized ATAC-Seq tracks from adult $GABA_A\alpha3$KO and littermate control (Ctrl) retinas showing promoter accessibility for the *Gabra1* locus. Red box highlights similar *Gabra1* promoter accessibility between genotypes.

See also Figures S6 and S7.

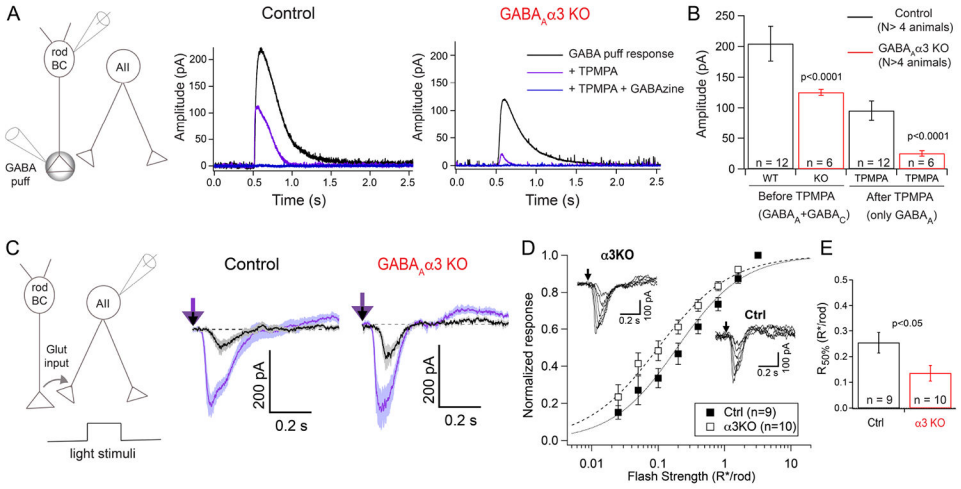

Figure 6: GABA$_A$-mediated response from GABA$_A$α3KO rod BC terminals is attenuated leading to increased AII sensitivity.

(A) Responses from adult rod BCs after GABA-puff application at their terminals. Exemplar trace depicting net GABA-evoked responses from GABA$_A$α3KO and littermate control (Control) rod BCs, and responses after application of the GABA$_C$R antagonist, TPMPA, and GABA$_A$R antagonist, GABAzine.

(B) Quantification of rod BC current amplitude before and after TPMPA application from adult GABA$_A$α3KO-Control retinas. Numbers within the histograms represent recorded cells in each condition.

(C) Exemplar recordings of responses to brief light flashes from an AII in adult GABA$_A$α3KO (*right*) and Control (*middle*) whole-mount retinas. Thick lines represent the average response (shaded region=SEM) to ten repeats of a dim flash (grey arrow/trace; 0.025 R*/Rod/flash) and a flash that was ~100 times brighter (purple arrow/trace; 3.2 R*/Rod/flash).

(D) Normalized flash responses across adult AIIs for Control (closed markers/Ctrl, N=5 animals) and GABA$_A$α3KO (open markers/α3KO, N=4 animals) retinas. *Insets:* Example responses to a range of flash strengths.

(E) Quantification of the flash strength at which the amplitude of the AII response reaches 50% of its maximum value ($R_{50\%}$) across adult GABA$_A$α3KO-Ctrl.

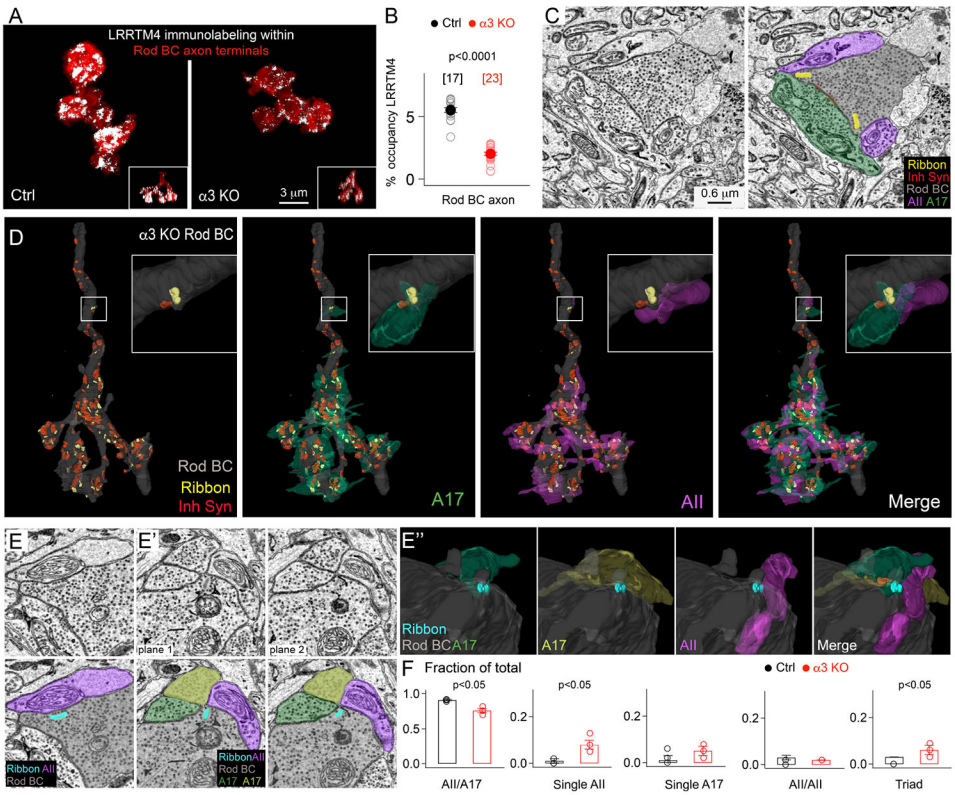

Figure 7: LRRTM4 is downregulated in GABA$_A$α3KO rod BC terminals with perturbed synaptic dyad arrangements.

(A) LRRTM4 immunofluorescence (white) localized within adult rod BC terminals (red) in a littermate control (Ctrl) and GABA$_A$α3KO retina. Insets show side-views.

(B) % occupancy of LRRTM4 within adult GABA$_A$α3KO-Ctrl rod BC boutons. N=4 animal pairs.

(C) Single-plane electron micrograph of an adult rod BC terminal in the GABA$_A$α3KO retina with two ribbon sites apposed to an A17 and an AII process characteristic of a normal dyad arrangement. The right panel is pseudo-colored for visualization of synaptic elements/ partners. A17->RBC inhibitory synapse denoted as Inh Syn.

(D) 3D view of an entire rod BC terminal (gray) from an adult GABA$_A$α3KO showing ribbons (yellow), inhibitory sites (red), AII (magenta) and A17 (green) partners at each ribbon. Inset shows magnified view of a ribbon synapse with dyad components.

(E-E") Single-plane electron micrograph of an adult GABA$_A$α3KO rod BC with ribbons mis-localized opposite a single AII process or present at a triadic arrangement with an AII and two different A17 processes. Bottom panels are pseudo-colored. **E"** is the 3D rendering of GABA$_A$α3KO triad arrangement shown in E'.

(F) Fraction of total rod BC ribbon sites with indicaed postsynaptic arrangements in adult wildtype-GABA$_A$α3KOs. (3 wildtype, 3 GABA$_A$α3KO reconstructions from 2 animal pairs). For AII/A17 arrangements, the values for GABA$_A$α3KO include AII/A17 dyads with lateral/horizontal and vertical ribbons. AII/A17 dyads with lateral ribbons were never observed in wildtype. Wildtype data from Sinha *et al.*[43].

See also Figure S6.

REAGENT or RESOURCE	SOURCE	IDENTIFIER
Antibodies		
Mouse monoclonal anti-PKC clone MC5	Sigma	Catalog # P5704; RRID:AB_477375
Rabbit polyclonal anti-VIAAT	Synaptic Systems	Catalog # 131003; RRID:AB_887869
Rabbit polyclonal anti-$GABA_A\gamma2$	Synaptic Systems	Catalog # 224003; RRID:AB_2263066
Guinea pig polyclonal anti-$GABA_A\beta3$	Synaptic Systems	Catalog # 224 404; RRID:AB_2619936
Rabbit polyclonal anti-Dsred	Clontech/Takara Bio	Takara Bio Cat# 632496; RRID:AB_10013483
Mouse monoclonal anti-RFP	Abcam	Catalog # ab65856
Rabbit polyclonal anti-lucifer yellow	Invitrogen	Catalog # A5750; RRID:AB_2536190
Mouse monoclonal anti-GlyR$\alpha1$	Synaptic Systems	Catalog # 146111; RRID: AB_887723
Rabbit polyclonal anti-$GABA_C$	[34]	Generated in Heinz Wässle and Joachim Bormann's Lab.
Guinea pig polyclonal anti-$GABA_A\alpha1$	[13]	Generated in Jean-Marc Fritschy's Lab
Guinea pig polyclonal anti-$GABA_A\alpha3$	[13]	Generated in Jean-Marc Fritschy's Lab
Rabbit polyclonal anti-LRRTM4 (BC262)	[56]	Generated in Ann Marie Craig's Lab
Mouse anti-$GABA_A\alpha1$	Neuromab	Catalog # 75-136; RRID:AB_2108811
Mouse anti-Actin	Chemicon/Millipore	Catalog # MAB1501; RRID:AB_2223041
Chemicals, peptides, and recombinant proteins		
Ames	Sigma	A1420
Lucifer yellow	Sigma	L0259
GABAzine (SR-95531)	Sigma	S106
TPMPA	Tocris	1040
GABA	Sigma	A2129
Alexa 594-hydrazide	Invitrogen	A10438
Alexa 488-hydrazide	Invitrogen	A10436
Vectashield antifade mounting medium	Vector Labs	Catalog# H-1000
M-MLV reverse transcriptase	Promega	M1701
Critical commercial assays		
DNA/RNA/Protein extraction kit	IBI Scientific	IB47702
PowerUp SYBR™ Green Master Mix	Applied Biosystems	A25741
Nextera DNA library prep kit	Illumina	FC-121-1030
Deposited data		
ATAC-seq $\alpha3$KO/control retina	This paper	GEO: GSE180163
Experimental models: Organisms/strains		
Mouse: $GABA_A\alpha3$ knockout	U. Rudolph[44]	N/A
Mouse: C57BL/6J	Jackson Labs	JAX Stock No: 000664
Mouse: *Grm6*-tdtomato	Rachel Wong[39]	N/A
Mouse: Ai9 reporter; B6.Cg-Gt(ROSA)26Sor$^{tm9(CAG-tdTomato)Hze}$/J strain	Jackson Labs	JAX Stock No: 007909

REAGENT or RESOURCE	SOURCE	IDENTIFIER
Mouse: *slc6a5*-Cre	Allen Brain Institute (GENSAT)	N/A
Mouse: *Grm6*-Cre	Rachel Wong[28]	N/A
Mouse: *Vsx1*-cerulean	Rachel Wong[28]	N/A
Mouse: $GABA_A\alpha1$ floxed; B6.129(FVB)-Gabra1^{tm1Geh}/J	Jackson Labs	JAX Stock No: 004318
Oligonucleotides		
GAPDH forward: GGCCGGTGCTGAGTATGTCG	[68]	N/A
GAPDH reverse: TTCTGGGTGGCAGTGATGGC	[68]	N/A
$GABA_A\alpha1$ Forward: CACCATGAGGTTGACCGTGA	This paper	N/A
$GABA_A\alpha1$ Reverse: CTACAACCACTGAACGGGCT	This paper	N/A
$GABA_A\alpha3$ Forward: GTGACACTCGATCTCACAGGT	This paper	N/A
$GABA_A\alpha3$ Reverse: ATATCTGGGGCATGCTTGGG	This paper	N/A
$GABA_C\rho$ Forward: GAGTTTCCCTGGGGATCACG	This paper	N/A
$GABA_C\rho$ Reverse: GCCATGGCTTGAACAGCATC	This paper	N/A
PCP2 Forward: CAGACCTTCTAGACAAGGCAGG	This paper	N/A
PCP2 Reverse: TCGTTTCTGCATTCCATCCTTG	This paper	N/A
Software and algorithms		
BEDtools (version 2.23.0)	[74]	https://github.com/arq5x/bedtools2
HOMER (version 4.6)	[73]	http://homer.ucsd.edu/homer/
Trimmomatic (version 0.33)	[71]	http://www.usadellab.org/cms/?page=trimmomatic
IGOR Pro	WaveMetrics	https://www.wavemetrics.com/
MATLAB	Mathworks	https://ch.mathworks.com/products/matlab
Symphony	Symphony-DAS	https://github.com/symphony-das
ImageJ	NIH	https://imagej.nih.gov/ij/
Amira	ThermoFisher Scientific	https://www.fei.com/software/amira/